Research Square

Preprints are preliminary reports that have not undergone peer review.
They should not be considered conclusive, used to inform clinical practice,
or referenced by the media as validated information.

# Loss of STARD7 triggers metabolic reprogramming and cell cycle arrest in breast cancer

**Alain Chariot**

alain.chariot@ulg.ac.be

University of Liege, GIGA-R https://orcid.org/0000-0002-1691-4347

**Ewelina Dondajewska**

University of Liege, GIGA-R

**Paula Allepuz-Fuster**

University of Liege, GIGA-R

**Chloé Maurizy**

University of Liege, GIGA-R

**Arnaud Blomme**

University of Liège https://orcid.org/0000-0003-4183-8726

**Pierre Close**

University of Liège

**arnaud lavergne**

University of Liege https://orcid.org/0000-0003-4817-3202

**Latifa Karim**

University of Liege, GIGA-R

**Marc Thiry**

**Ivan Nemazanyy**

https://orcid.org/0000-0001-8080-839X

**Roopesh Krishnankutty**

**Jair Marques Junior**

University of Edinburgh

**Alex von Kriegsheim**

University of Edinburgh https://orcid.org/0000-0002-4952-8573

**Nate Henneman**

**Ganna Panasyuk**

**Kateryna Shostak**

University of Liege https://orcid.org/0000-0002-9946-3536

**Article**

**Keywords:**

**Posted Date:** July 3rd, 2024

**DOI:** https://doi.org/10.21203/rs.3.rs-4582125/v1

**License:** This work is licensed under a Creative Commons Attribution 4.0 International License.
Read Full License

**Additional Declarations:** There is **NO** conflict of interest to disclose.

# Abstract

Cancer cells adapt their metabolism to support aberrant cell proliferation. However, the functional link between metabolic reprogramming and cell cycle progression remains largely unexplored. Mitochondria rely on the transfer of multiple lipids from the endoplasmic reticulum (ER) to their membranes to be functional. Several mitochondrial-derived metabolites influence cancer cell proliferation by modulating the epigenome. Here we show that the loss of STARD7, a lipid transfer protein whose expression is enhanced in breast cancer, leads to a metabolic reprogramming characterized by the accumulation of Carnitine derivatives and S-Adenosyl-L-methionine (SAM). Elevated SAM levels causes the increase of H3K27 trimethylation on many gene promoters coding for candidates involved in cell cycle progression. Likewise, STARD7 deficiency triggers cell cycle arrest and impairs ERa-dependent cell proliferation. EGFR trafficking to lysosomes is also deregulated in breast cancer cells lacking STARD7. Therefore, mitochondria rely on STARD7 to support cell cycle progression in breast cancer.


# INTRODUCTION

The maintenance of membrane homeostasis relies on an intense exchange of lipids between cellular membranes [1]. Most lipids are synthesized within the endoplasmic reticulum (ER) and redistributed from there to other cellular membranes, including mitochondrial membranes. Mitochondria carry out several essential functions, such as ATP production, calcium regulation and redox homeostasis [2,3].

STARD7, a lipid transfer protein belonging to the family of START (steroidogenic acute regulatory protein-related lipid transfer) domain superfamily, facilitates the transfer of lipids among intracellular membranes [4]. STARD7 preferentially binds to phosphatidylcholine (PC) and promotes the delivery of PC to the mitochondria [5]. Consistently, STARD7-deficient cells show a reduction of mitochondrial PC as well as a disorganized cristae structure of mitochondria [6]. This altered mitochondrial structure is associated with a decreased aerobic respiration, increased oxidative stress and mitochondrial DNA damage, resulting in altered barrier integrity in vivo [7]. STARD7 is actually localized in the intermembrane space and mitochondrial STARD7 is necessary and sufficient for PC accumulation in the inner membrane as well as for mitochondrial respiration and cristae morphogenesis [8]. The inner membrane protease PARL (presenilin-associated rhomboid-like) can cleave STARD7, resulting in the release of mature STARD7 in the cytosol [8]. Interestingly, cytosolic STARD7 is critical for the transport of Coenzyme Q, a redox-active lipid acting as an universal electron carrier in the mitochondrial respiratory chain, to the plasma membrane and consequently protects from ferroptosis, suggesting that STARD7 function is not limited to PC transport [9].

Members of the START protein family are aberrantly expressed in cancer. Indeed, STARD1, which promotes cholesterol trafficking to mitochondria, is overexpressed in non-alcoholic steatohepatitis (NASH)-derived hepatocellular carcinoma (HCC) and critically contributes to HCC in mice [10]. STARD3, another cholesterol-binding protein, is part of the amplified locus with ERBB2 on human chromosome

17q12 found in both gastric and breast cancer [11]. STARD3 contributes to breast cancer development, at least by promoting both Src and PI3K/AKT/mTOR activation [12,13]. STARD4, which facilitates the transfer of cholesterol to the cytoplasmic membrane, is overexpressed in breast cancer and promotes cell proliferation and migration [14]. Finally, STARD10 is also overexpressed in breast cancer and cooperates with ErbB receptor signaling in cellular transformation [15]. Likewise, ethanol abuse, which exacerbates breast cancer progression, induces both STARD10 and ERBB2 expression [16]. Therefore, these studies undoubtedly established a link between aberrant expression of START protein family members and cancer development but underlying molecular mechanisms have not been extensively dissected yet.

We demonstrate here that STARD7 is overexpressed in ERα$^{+}$ breast malignancies and in Triple Negative Breast Cancers (TNBCs). Loss of STARD7 in breast cancer cells causes a metabolic reprogramming characterized by the accumulation of several mitochondrial metabolites, including carnitine derivatives and S-Adenosylmethionine (SAM). The defective transport of PC to mitochondria due to STARD7 deficiency also leads to increased numbers of mitochondria-associated ER membranes (MAMs). Accumulation of SAMs in breast cancer cells lacking STARD7 enhances H3K27 methylation on genes coding for candidates involved in cell cycle progression. Loss of STARD7 consequently causes cell cycle arrest, at least through defective ERα- and EGFR-dependent signaling pathways as well as autophagy. Collectively, our results provide molecular mechanisms through which cancer cells reprogram their metabolic and transcriptomic signatures to support sustained cell proliferation.

# MATERIAL AND METHODS

## Cell lines and reagents

Unless stated otherwise, MCF7, MDAMB231, HCC1569 and LentiX cells were cultured in DMEM high glucose (Lonza) + 10% Fetal Bovine Serum (Gibco), 1% Penicillin/Streptomycin (Lonza). T47D cell were cultured in RPMI (BioWest) + 10% FBS, 1% Penicillin/Streptomycin. hTERT-RPE1 retinal cells were cultured in DMEM/F12 (Gibco) + 10% FBS, 1% Penicillin/Streptomycin. All cells were maintained in a 37°C incubator in 95% humidity and 5% $CO_2$.

For estrogens (E2) treatments, control and STARD7-depleted MCF7 or T47D cells on D4 post transduction were first seeded in 6 well plates in DMEM:F12 without phenol red (Gibco), supplemented with 5% of charcoal/dextran treated FBS (HyClone) and 1% of Penicillin/Streptomycin for 48 hours as a pre-treatment to deplete hormones. Afterwards, the medium was changed to a medium with β-Estradiol (E2) (10 nM) (Sigma-Aldrich, E2257) and cells were harvested at the indicated time points (for protein lysates, 30, 60 minutes, 24 and 48 hours), RNA extraction (6 hours) and EDU proliferation analysis (24 and 48 hours). For EGF treatments, cells were first serum-starved overnight or for 24 hours in a medium with 0% FBS before the addition of EGF (100 nM) (Cell Signaling, #9908). Treatments with Chloroquine (25 µM) (Sigma-Aldrich), C6628-25) and Rapamycin (20 nM) (LC Laboratories, R-5000) were carried out

for 24 hours with cells cultured in DMEM high glucose (Lonza) + 10% Fetal Bovine Serum (Gibco), 1% Penicillin/Streptomycin (Lonza).

# Lentiviral vector production and cell transduction

Transfection mixture was prepared in 800 µL OptiMEM (Gibco) by adding following plasmids: 12 µg of psPAX2 (AddGene #12260), 5 µg of pVSV-G (AddGene #138479) and 12 µg of expression vector carrying shRNA sequence, in the presence of 80 µL of TransIT-*LT1* Transfection Reagent (Mirus, Mir2360). Expression vectors were: pLVshCtrl (Sigma, SHC002), pLVshSTARD7#2 (Sigma, TRCN000028081) and pLVshSTARD7#4 (Sigma, TRCN0000155648). After 15 minutes of incubation at room temperature, the transfection mixture was added dropwise on top of the 50–60% confluent LentiX cells on T75 $cm^3$. Medium was changed within 6–16 hours, with 8 mL of a complete culture medium. After 72 hours of viral particle production, medium with LV was collected, centrifuged at 800 x g for 10 minutes, 0.22 µL filtered and either added directly to cells to be transduced or frozen in -80°C.

For cell transduction, on day 0 (D0), cells were transduced using the medium containing lentiviral particles in the presence of 8 µg/mL of Polybrene transfection reagent (Millipore). After 24 hours (D1), the medium was changed to the selection medium with 1 µg/mL Puromycin (InVivoGen) for 48 hours. Afterwards (D3-D4), cells were split using the Trypsin/EDTA solution (BioWest) and seeded for experiments. All experiments were done on D5-D6 post transduction.

# Real-Time PCR analyses

Total RNAs were extracted from cultured cells using the column based extraction E.Z.N.A.® Total RNA Kit I (Omega Biotek) according to manufacturer's protocol. cDNAs were obtained using the RevertAid H Minus First Strand cDNA Synthesis Kit using oligo(dT)18 primers and 1 µg of total RNAs as a template. Real-time PCR reactions were carried out on Light Cycler480 (Roche) with TB Green Premix Ex Taq II Tli RNase H Plus (Takara Bio) and specific primers designed with the PrimerBlast software (NCBI). Primer sequences can be found in Table 1. Ct values were used to calculate fold change of expression using the $2^{-\Delta\Delta Ct}$ method. HSP90B1, GAPDH, and β-Actin were used as housekeeping controls.

Table 1

| | |
|---|---|
| **GAPDH** | **F : GCATCTTCTTTTGCGTCGC** |
| | **R : CCAAATGCGTTGACTCCGA** |
| HSP90B1 | F : CTGTATTCAGGCCCTTCCCG |
| | R : ACCACAGCCTTTTCAATCTTGT |
| ACTB | F : AGAGCTACGAGCTGCCTGAC |
| | R : AGCACTGTGTTGGCGTACAG |
| STARD7 | F : ATTCAGAGGGCAAAGAGCAA |
| | R : AAGGTGGGTGCCTGTAATTG |
| ESR1 | F : GATCAACTGGGCGAAGAGGG |
| | R : CATTTTCCCTGGTTCCTGTCC |
| CCND1 | F : ATCAAGTGTGACCCGGACTG |
| | R : CTTGGGGTCCATGTTCTGCT |
| CCNB1 | F : CTGCTGGGTGTAGGTCCTTG |
| | R : AGCTGAAGGTTTTGCTTCCTTC |
| PLK1 | F : CCGCAATTACATGAGCGAGC |
| | R : GCTTGGTGTGATCCTGGAAGA |
| IGFBP4 | F : GCAGAAGCACTTCGCCAAAA |
| | R : CTCTCGAAAGCTGTCAGCCA |
| RARA | F : CACACACCTGAGCAGCATCAC |
| | R : CGGTCCTTTGGTCAAGCAGT |
| AURKA | F : GTGGGGGATATCTCAGTGGC |
| | R : ATGGAGTGAGACCCTCTAGC |
| PTGS2 | F : TGCGCCTTTTCAAGGATGGA |
| | R : ACATCATCAGACCAGGCACC |
| MYBL2 | F : CAGCCACTTCCCTAACCGCA |
| | R : TGTCCACTGCTTTGTGCCAT |
| MYC | F: CCGCTTCTCTGAAAGGCTCT |
| | R: CTAACGTTGAGGGGCATCGT |
| ERBB2 | F : AGCTCATCTACCAGGAGTGG |

| | |
|---|---|
| **GAPDH** | **F : GCATCTTCTTTTGCGTCGC** |
| | **R : CCAAATGCGTTGACTCCGA** |
| | R : GGTCACCATCAAATACATCGGA |
| ERBB3 | F : TCAGAGTCATCAGAGGGGCA |
| | R : CCACTGAAGAAAGGGTGCCT |
| MMP9 | F : CGACGTCTTCCAGTACCGAG |
| | R : TTGTATCCGGCAAACTGGCT |
| CFAP69 | F : AACTGTGTGGCTTGCCATTT |
| | R : GCTTCTTTGGTGGTTCTGCAT |
| DNAH1 | F : AGATGGCCGTTATCTGGCTC |
| | R : CACGCTTTATCCAGTGTCGC |
| WDR19 | F : TCCGCTTGTACATGGCTCTG |
| | R : GGCCATCTCGGAGGGAATTT |
| IFT43 | F : ACAGCTGGATCTGAACGCAT |
| | R : TCCAGGTCACGGTAGGTCAT |
| PLA2G3 | F : GGCCTAAAACCTCAGGGTGC |
| | R : AGCATGTTGGTAACCTCGGG |
| IFT22 | F : TGTGGTGGCGATGCTAAGTT |
| | R : TTCAAGGGTGGCGACAAAGA |
| DNAAF4 | F : GGCACATGTACGACGTGGA |
| | R : TTCATAATCCTGTAGGCCTTCTAC |
| EGFR | F : CTGTGCCATCCAAACTGCAC |
| | R : CGATGGACGGGATCTTAGGC |
| SRC | F : TCACCGCAAGAGCTACCATT |
| | R : TCCTGGGAAGGTTGGAACTG |
| CBL | F : AGCTCGGCTCCAGAAATTCA |
| | R : CCAATAGCCCACTGACCCAG |
| RB1 | F : AGGTCTGCCAACACCAACAA |
| | R : GCATTCGTGTTCGAGTAGAAGTC |

# Transcriptomic analyses by RNA sequencing

RNA sequencing was performed on libraries prepared from total RNA samples from MCF7 cells (shControl, shSTARD7#2, shSTARD7#4). Three biological replicates were analysed for each condition. Total RNAs were extracted by using the E.Z.N.A.® Total RNA Kit (Omega Bio-tek) according to the manufacturer's protocol. Total RNAs before elution were treated with TURBO™ DNase (ThermoFisher Scientific, AM2238). RNA integrity was verified on a Bioanalyser 2100 with RNA 6000 Nano chips (Agilent technologies). RNA integrity number score was above 9 for every sample. Libraries were prepared using Truseq® stranded mRNA Sample Preparation Kits (Illumina) following manufacturer's instructions. Libraries were validated using QIAxcel Advanced System and quantified by qPCR using the KAPA library quantification kit. Libraries were multiplexed and sequenced on an Illumina NextSeq500 sequencer to generate more than ~ 25,000,000 paired-end reads (2 × 150 bases) per library. Raw reads were demultiplexed and adapter-trimmed using Illumina bcl2fastq conversion software v2.20. Reads were processed within the nf-core/rnaseq-1.4.2 pipeline [17] using STAR aligner, the human reference genome GRCh38 and the gene annotations from Ensembl release 97. Quality of the sequencing data was successfully controlled using QC modules of the pipeline and a report has been compiled with MultiQC. The data has been deposited to the Genomic Expression Omnibus (GEO) with the following accession number : GSE251873.

# SDS-PAGE and western blot analyses

Cells were washed twice in ice-cold PBS and scrapped in an ice-cold RIPA lysis buffer (50 mM Tris-HCl pH 7.4, 2 mM EDTA, 50 mM NaF, 150 mM NaCl, 0.1% SDS, 0.5% sodium deoxycholate, 1% NP40) supplemented with cOmplete Protease Inhibitor (Roche) and PhosStop (Roche). Lysates were cleared by centrifugation 15 minutes, 15 000 x g at 4°C and protein concentrations were measured using the Pierce BCA Protein Assay Kit (Thermo Scientific) according to manufacturer's instructions. Samples were denaturated by boiling for 7 minutes in a Laemmli Buffer with β-mercaptoethanol and 20 µg of total proteins were loaded per well of SDS-PAGE gel (8–14%). Samples were separated under reducing conditions and transferred to PVDF membrane (Immobilion-P, Millipore), using wet transfer chambers. Membranes were blocked in 5% skimmed milk for 45 minutes, cut and incubated with primary antibodies overnight on rotor at 4°C. A list of primary antibodies is available in Table 2. The following day, membranes were washed five times in TBS-T and incubated for 1 hour at room temperature with HRP conjugated secondary antibodies donkey anti-rabbit (GE Healthcare, NA934V) or sheep anti-mouse (GE Healthcare, NA931V). After subsequent five washing steps, membranes were visualized with the Pierce ECL Western (Thermo Scientific) or SuperSignal West Femto Maximum Sensitivity Substrate (Thermo Scientific) on the ImageQuant LAS 4000 mini (GE Healthcare).

Table 2

| Name of antibody | Reference number | Company |
|---|---|---|
| GAPDH (D16H11) | #5174 | Cell Signaling Technologies |
| STARD7 | PAS-30772 | Invitrogen |
| ACTIN-HRP (AC-15) | A3854 | Sigma |
| Mitofusin2 (D2D10) | #9482 | Cell Signaling Technologies |
| FIS1 | HPA017430 | Sigma |
| DRP1 (C-5) | sc-271583 | Santa Cruz |
| Tri-Methyl-Histone H3 (Lys27) (C36B11) | #9733 | Cell Signaling Technologies |
| Tri-Met-H3K4 | Ab12209 | Abcam |
| Ac-H3K27 | A7253 | AbClonal |
| Met-H3K9 Trimethyl Histone H3 (6F12-H4) | sc-130356 | Santa Cruz |
| Histone H3 | ab1791 | Abcam |
| Cyclin A (B-8) | sc-271682 | Santa Cruz |
| Cyclin B1 | A305-000A | Bethyl Laboratories Inc. Montgomery, TX, USA |
| Cyclin B2 | A304-509A | Bethyl Laboratories Inc. Montgomery, TX, USA |
| Cyclin D1 (92G2) | #2978 | Cell Signaling Technologies |
| Cyclin E (E-4) | sc- 377100 | Santa Cruz |
| P21 Waf/Cip1 (12D1) | #2947 | Cell Signaling Technologies |
| P27 Kip1 (D69C12) | #3686 | Cell Signaling Technologies |
| MYC (D84C12) | #5605 | Cell Signaling Technologies |
| ERalpha (HC-20) | sc-543 | Santa Cruz |
| SOX9 | AB5535 | |
| EGFR (A-10) | Sc-373746 | Santa Cruz |
| Phospho-ERalpha (S118) | #16J4 | Cell Signaling Technologies |
| HER2/ErbB2 (29D8) | #2165S | Cell Signaling Technologies |
| HER3/ErbB3 (D22C5) | #12708S | Cell Signaling Technologies |

| Name of antibody | Reference number | Company |
|---|---|---|
| Phospho-EGFR (Y1068) | #3777 | Cell Signaling Technologies |
| TrxR1 (B-2) | sc-28321 | Santa Cruz |
| TXNIP (D5F3E) | #14715 | Cell Signaling Technologies |
| LAMP1 (D401S) | #15665 | Cell Signaling Technologies |
| LAMP2 (H4B4) | sc18822 | Santa Cruz |
| PERK (C33E10) | #5683 | Cell Signaling Technologies |
| pAKT (S473) (D9E) | #4060 | Cell Signaling Technologies |
| LC3B (D11) | #3868 | Cell Signaling Technologies |
| p62 | NBP1-48320 | Novus |
| Rab11 | #3539 | Cell Signaling Technologies |

# Immunofluorescence analyses

To measure the length of the primary cilium, hTERT-RPE1 cells were kept in DMEM/F12 medium supplemented with 10% FBS and 1% pen/strep in an incubator with a 5% CO2 and 95% humidified atmosphere. hTERT-RPE1 cells were transduced with the LV-sh Control (CTRL), LV-sh STARD7#2 or LV-sh STARD7#4 construct and the medium was changed to medium containing 1 µg/ml of puromycin for 48 hours. After that, cells were split and seeded for experiments. Three days after transduction, cells were seeded on coverslips. Four days after transduction, cells were starved with no serum Optimem for 48 hours. Cells were fixed in 4% PFA on day six after transduction, blocked, permeabilized and stained with a mouse anti-Arl13b antibody overnight. The next day, coverslips were incubated with a secondary goat anti-mouse IgG AlexaFluor568 antibody and DAPI and mounted. Samples were visualized using a Zeiss HR LSM 880 confocal microscope. A Z stack of 4 µm was taken for each condition. Data was analysed using the Imaris software. 6 images of cells transduced with the LV-sh CTRL construct were analysed (measurements: n = 12) and 9 images of cells transduced with the LV-shRNA STARD7 construct (3 images of with cells transduced with the shRNA STARD7#2 construct, measurements: n = 10, 6 images of cells transduced with the shRNA STARD7#4 construct, measurements: n = 15). Statistical significance was determined with the unpaired Student T-test, ** = $p < 0.01$.

To assess EGFR trafficking upon EGF stimulation, control or STARD7-depleted MDA-MB231 cells were seeded on coverslips in 6-well plates and serum-starved for 24 hours. Cells were subsequently untreated or stimulated with EGF (Alexa Fluor® 488 EGF complex, Life Technologies, Grand Island, NY). Cells were kept for 45 minutes at 4°C in the dark, put back at 37°C for 10 minutes, washed with some fresh medium to remove EGF and incubated again at 37°C for 15 or 30 minutes. Cell were then fixed with paraformaldehyde 4% and preimmobilized with Triton X 0.3% for 10 minutes at room temperature. They

were subsequently incubated with an anti-EEA1 antibody for 2 hours at room temperature followed by 45 minutes of incubation at room temperature with an Alexa Fluor 594-conjugated antibody (Dako, Glostrup, Germany). Images were acquired with the confocal system of Leica SP5 inverted microscope.

To assess autophagy, cells were seeded on coverslips in 6-well plates. After transfection or treatment, cells were washed in PBS, fixed with 4% paraformaldehyde (PFA) in PBS for 15 minutes and pre-immobilized with 0.2% Triton-X100/PBS for 10 minutes at room temperature. Cells were then washed and blocked for 1 hour (5% BSA + 5% normal goat serum in PBS) followed by overnight incubation at 4°C with primary antibodies in a blocking solution. The next day after 1 hour incubation with appropriate goat secondary antibodies coupled to Alexa Fluor 488 or 568 fluorophores (Life Technologies), coverslips were washed and incubated 10 minutes with DAPI (Life Technologies). ProLong (Life Technologies) was used for mounting on glass slides and images were acquired with the Leica TCS SP5 II confocal system (Leica Microsystems, Wetzlar, Germany).

# Proliferation analyses

Cell proliferation was measured by the incorporation of thymidine analogue EdU into newly synthesized DNAs by using the Click-iT™ EdU Alexa Fluor™ 488 Flow Cytometry Assay Kit (Invitrogen ref: C10420) according to manufacturer's protocol. Briefly, cells were incubated with 10 µM EdU in complete medium for 2 hours. Following washing and harvesting by trypsinization, cells were fixed in Click-iT® fixative for 15 minutes and permeabilized by the saponin-based buffer. Cells were incubated with Click-iT® reaction cocktail for 30 minutes at room temperature. Following washing steps, samples were analysed on the FACS Canto (BD Biosciences) at the 488 nm excitation laser with a green emission filter. Results were analyzed with the FlowJo software.

# Targeted LC-MS metabolomics analyses

MCF7 cells were transduced with lentiviral vectors (shControl, shSTARD7#2 and shSTARD7#4) in 6-well plates and after selection in a Puromycin-containing medium for 5 days, cells were washed with cold PBS, scrapped, centrifuged and pellets were kept frozen in liquid nitrogen. For metabolomic analyses, the extraction solution was composed of 50% methanol, 30% acetonitrile (ACN) and 20% water. The volume of the extraction solution was adjusted to cell number (1 ml per $10^6$ cells). After addition of the extraction solution, samples were vortexed for 5 minutes at 4°C and centrifuged at 16,000*g* for 15 minutes at 4°C. The supernatants were collected and stored at -80°C until analysis. LC/MS analyses were conducted on a QExactive Plus Orbitrap mass spectrometer equipped with an Ion Max source and a HESI II probe coupled to a Dionex UltiMate 3000 uHPLC system (Thermo). External mass calibration was performed using a standard calibration mixture every seven days, as recommended by the manufacturer. The 5 µl samples were injected onto a ZIC-pHILIC column (150 mm × 2.1 mm; i.d. 5 µm) with a guard column (20 mm × 2.1 mm; i.d. 5 µm) (Millipore) for LC separation. Buffer A was 20 mM ammonium carbonate, 0.1% ammonium hydroxide (pH 9.2) and buffer B was ACN. The chromatographic gradient was run at a flow rate of 0.200 µl $min^{-1}$ as follows: 0–20 min, linear gradient from 80–20% of buffer B; 20–20.5 min, linear gradient from 20–80% of buffer B; 20.5–28 min, 80% buffer B. The mass

spectrometer was operated in full scan, polarity switching mode with the spray voltage set to 2.5 kV and the heated capillary held at 320°C. The sheath gas flow was set to 20 units, the auxiliary gas flow to 5 units and the sweep gas flow to 0 units. The metabolites were detected across a mass range of 75–1,000 *m/z* at a resolution of 35,000 (at 200 *m/z*) with the automatic gain control target at $10^6$ and the maximum injection time at 250 ms. Lock masses were used to ensure mass accuracy below 5 ppm. Data was acquired with Thermo Xcalibur software (Thermo). The peak areas of metabolites were determined using Thermo TraceFinder software (Thermo), identified by the exact mass of each singly charged ion and by the known retention time on the HPLC column.

# Subcellular Fractionations

Cytoplasmic and crude mitochondrial fractions were separated using the Mitochondrial Isolation Kit for Cultured Cells (Thermo Scientific) according to manufacturer's protocol. Briefly, cells from 15 cm culture dishes were scrapped on ice and pelleted by centrifugation 850 x g for 2 minutes. 800 µL of Reagent A with protease inhibitors was added, samples were vortexed for 5seconds and incubated on ice for 2 minutes. Afterwards, 10 µL of reagent B was added and samples were vortexed at max speed for 5 seconds and incubated on ice for 5 minutes with vortexing every minute. 800 µL of reagent C was added, and after centrifugation steps, supernatants - cytosolic fractions -were transferred to a fresh tube. 500 µL of reagent C was added to the remaining pellet and after centrifugation, the crude mitochondrial fraction was obtained. For western blot analyses, mitochondrial pellets were suspended in 2% CHAPS in TBS. For MAMs isolation, all subsequent steps were carried out as previously described [18].

# Transmission Electron Microscopy

Cells were fixed for 1 hour at 4°C in a solution composed of 2.5% glutaraldehyde in 0.1 M Sorensen's buffer (0.2 M $NaH_2PO_4$, 0.2 M $Na_2HPO_4$, pH 7.4). After several washes in the same buffer, the samples were post-fixed for 60 minutes with 2% osmium tetroxide, washed in deionised water, dehydrated through graded ethanol (70, 95, and 100%) and embedded in epon for 48 hours at 60°C. Ultrathin sections (700-A thick) were obtained by means of an ultramicrotome (Reichert Ultracut E) equipped with a diamond knife. The ultrathin sections were mounted on palladium/copper grids coated with collodion and contrasted with uranyl acetate and lead citrate for 5 minutes each before being examined under a Jeol JEM1400 transmission electron microscope at 80 kV. Random fields were photographed using an 11-megapixel camera system (Quemesa, Olympus). Morphometric measurements were performed with iTEM v5.2 (Olympus, Tokyo, Japan) and analyzed using Image J v1.52a software.

To evaluate the area occupied by mitochondria in control or STARD7-depleted cells, we randomly took 22 images of whole cells from each sample with a JEOL 1400 TEM at × 2,500 magnification. In each image, we counted the number of mitochondria (651 in control cells and 393 in STARD7-depleted cells for a total of 1044 mitochondria) and calculated the average number of mitochondria on the cytoplasmic area examined on each cell incidence and the average area occupied by the mitochondria on each cell incidence. In addition, we assessed the configuration of 5 mitochondria in 21 control cells and in 22 STARD7-depleted cells, respectively.

To evaluate the frequency of contact between the mitochondria and the ER in control or STARD7-depleted cells, we randomly took 20 images of cytoplasmic area from 21 different cells in each sample with a JEOL 1400 TEM at ×10,000 magnification. In each image, we counted the number of mitochondria (488 in control cells and 347 in STARD7-depleted cells for a total of 835 mitochondria) and calculated the proportion of mitochondria in close contact with ER (< 30 nm). Moreover, the perimeter of each mitochondria and the proportion of the mitochondrial surface closely associated with ER were calculated.

# Proteomic analyses

Pellets were resuspended in 50 µl 6 M guanidine hydrochloride 100 mM Tris pH8 .5 containing 1.5 mg/mL TCEP and 1 mg/mL chloroacetamide and digested with 1 µg LysC (FUJIFILM Wako Pure Chemicals U.S.A. Corporation) for 4 hours at 37°C. Subsequently, samples were diluted to 300 µl with LC-MS Water and digested overnight using 1 µg of porcine Trypsin (Thermo Scientific) followed by desalting using stage-tips before MS analyses. Peptides were resuspended in 0.1% TFA in Water and peptide content was estimated 280nm Absorption using a Nanodrop 2000 (Thermo Scientific). 1 µg was then injected and separated on an Ultimate 3000 Nano using a C18 packed emitter (Aurora, IonOptiks, Australia), with a gradient from 4–29% acetonitrile in 90 minutes, with a 10 minutes 80% wash. 0.5% acetic acid was present throughout. Peptides were analysed in data-independent acquisition (DIA) mode on a Thermo Fusion Lumos. The mass spectrometer was operated in DIA mode, acquiring a MS 350–1650 Da at 120 k resolution followed by MS/MS on 45 windows with 0.5 Da overlap (200–2000 Da) at 30 k with a NCE setting of 27. Data was searched using DIA-NN (1.8.1) against the Uniprot Human database using the default setting for library-free search. The mass spectrometry proteomics data have been deposited to the ProteomeXchange Consortium via the PRIDE [1] partner repository with the dataset identifier PXD046984.

# H3K27Me3 ChIP Sequencing analyses

Samples for chromatin immunoprecipitation were prepared using an iDeal ChIP-seq Kit *for* Transcription Factors (Diagenode, Belgium) and according to manufacturer's instructions. Briefly, 3 x $10^6$ cells (MCF7 shControl and shSTARD7#2) were fixed by directly adding the crosslinking reagent to the medium on the cell culture plate. After 15 minutes of fixation at room temperature, the reaction was stopped with Glycine. Cells were washed with PBS on ice and scrapped in the lysis buffer (1 x $10^6$ cells /mL). After subsequent lysis steps, samples were immediately subjected to chromatin shearing using Bioraptor Plus (Diagenode) for 20 cycles (30 seconds "ON", 30 seconds "OFF") each at High power setting. ChIP of H3K27Me3 (Cell Signaling Technology (C36B11) Rabbit mAb #9733) was conducted on sheared protein from three independent experiments using the magnetic beads system. After elution, de-crosslinking and DNA purification, the library for sequencing was prepared. Next-generation sequencing was performed on all immunoprecipitated DNA samples and their respective inputs, with a depth of 50 mln clusters per sample. For data analysis, clean reads were aligned to the hg38 human genome using Bowtie2 version 2.4.4 and SAMtools version 1.13 was used to index and sort binary alignment map (BAM) files [19,20]. Heatmaps were generated using the deepTools2 plotHeatmap function [21]. Peak calling

was performed for all samples using MACS2 version 2.2.7.1 [22] with the following parameter: callpeak -t file_merged.bam -c file_inp.sorted.bam -f BAMPE -g hs -n file_merged --broad --outdir peaks; peaks were annotated, and pathway analysis performed using ChIPseeker and clusterProfiler, respectively [23,24] in R v4 1.2 (http://www.r-project.org/foundation/).

# FACS analyses

For the analysis of the lysosomal compartment, a cell-permeable fluorescent dye LysoTracker Red DND-99 (Invitrogen) was used. On day 5 post transduction, cells were washed with PBS, and detached from a 6 well culture plate using trypsin-EDTA solution. Trypsin was inactivated by the addition of a culture medium with FBS. Cells were spinned down and suspended in a full culture medium containing Lysotracker dye in final concentration of 100 nM and incubated at 37°C for 30 minutes. Afterwards, cells were centrifuged and suspended in PBS for the analysis on the FACS Fortessa (BD). Analysis was performed using an excitation laser 561 nm and fluorescence was collected on the PE channel. Data was analysed using the FlowJo software.

# Statistical Analysis

For all analyses in which three groups were compared (sh Control, sh STARD7#2 and sh STARD7#4), statistical significance was measured by one-way ANOVA for repeated measures, using the Dunnett's multiple comparison test, unless stated otherwise. When only two groups were compared (sh Control, sh STARD7#2), a student's t-test was employed. All analyses were done using the Prism software. Significance: * = $p < 0.05$, ** = $p < 0.01$, *** = $p < 0.001$, **** = $p < 0.0001$.

## RESULTS

# STARD7 is overexpressed in breast cancer

To learn more on mechanisms through which lipid transfer proteins regulate tumor development, we first looked at the expression profile of STARD7 in human tumors. STARD7 was overexpressed in many human tumors, including cholangiocarcinoma (CHOL), cervical squamous cell carcinoma and endocervical adenocarcinoma (CESC), diffuse large B cell lymphoma (DLBCL), glioblastoma (GBM), pancreatic adenocarcinoma (PAAD), rectum adenocarcinoma (READ), skin cutaneous melanoma (SKMC), testicular germ cells tumor (TGCT), thymoma (THYM) and breast cancer (BRCA), as indicated by data generated by the TCGA Research Network (https://www.cancer.gov/tcga) (Fig. 1A). STARD7 transcripts were indeed enriched in breast tumors versus normal adjacent tissues (Figs. 1B and 1C). Interestingly, mRNA levels of STARD7 were found elevated in benign breast neoplasms as well as in both ductal and invasive carcinomas when compared to levels in normal breast, suggesting that STARD7 overexpression occurs early during tumor development (Fig. 1D). The enrichment of STARD7 transcripts in tumors versus normal adjacent tissues was more pronounced in triple negative breast cancers (TNBCs) than in $ER^+$ malignancies (Fig. 1E). STARD7 overexpression was also detected at the protein

level in all tested clinical cases of TNBCs as well as in most $ER^+$ tumors (Fig. 1F). Therefore, breast cancer development is characterized by elevated levels of STARD7.

# Loss of STARD7 in breast cancer cells leads to changes in mitochondrial morphology

To define the biological processes controlled by STARD7 in breast cancer, we first generated MCF7 cells lacking STARD7. As PC transfer from the ER to mitochondria relies on STARD7, we looked at the consequences of STARD7 deficiency in both the shape and function of mitochondria. MCF7 cells lacking STARD7 had less but enlarged mitochondria (Fig. 2A). Moreover, MCF7 cells lacking STARD7 exclusively showed orthodox mitochondria while control cells showed 39% of condensed organelles, which have a contraction of the matrix space (Fig. 2B). To clarify whether the increased size and decreased number of mitochondria were the result of increased mitochondria fusion, we next looked at levels of key mitochondria dynamics regulators. In this context, levels of Mitofusin 2, a key protein in mitochondrial fusion, Dynamin-Related Protein 1 (DRP1), a dynamin-related GTPase involved in mitochondrial division as well as Mitochondrial Fission 1 (FIS1) involved in mitochondrial outer membrane fission [25–27] remained unchanged upon STARD7 deficiency (Fig. 2C).

Given the fact that STARD7 deficiency changes both mitochondrial number and size and because STARD7 promotes the transport of PC from the ER to mitochondria, we next looked at mitochondria-ER contacts. We observed that cells lacking STARD7 displayed more contacts between both organelles (Fig. 2D). Moreover, the percentage of mitochondrial perimeter in contact with the ER also increased upon STARD7 deficiency (Fig. 2D). Therefore, loss of STARD7 leads to higher numbers of mitochondria-associated membranes (MAMs) in breast cancer cells, potentially as a compensatory mechanism of a defective PC transport between both organelles.

We biochemically fractionated extracts from both control and STARD7-depleted MCF7 cells and noticed that IRE1α, an ER stress sensor also acting as a structural determinant of MAMs involved in the control of mitochondrial calcium uptake, but not BIP levels, increased in MAMs from STARD7-depleted cells (Fig. 2E). Of note, IRE1α levels also increased in additional cell compartments, including in both cytoplasmic and mitochondrial extracts (Fig. 2E). As expected, Sarcoplasmic/endoplasmic reticulum $Ca^{2+}$-ATPase 2b (SERCA2b) was enriched in MAMs from MCF7 cells [28] but its level did not dramatically change upon STARD7 deficiency (Fig. 2E). Moreover, Inositol 1,4,5-trisphosphate receptors (IP3R), Voltage-dependent anion channel 1 (VDAC1) and Glucose-regulated protein 75 (GRP75), which all form a complex to modulate ER-mitochondria Calcium [29], signaling, were also found in MAMs from MCF7 cells (Fig. 2E). However, although both GRP75 and IP3R levels in MAMs did not change upon STARD7 deficiency, MCF7 cells lacking STARD7 showed dramatically decreased levels of VDAC1 in MAMs but not in other cell compartments (Fig. 2E). This conclusion also applied to COX4 (Fig. 2E). Consistently, levels of IRE1α, another candidate found in MAMs [30], were elevated in total extracts from T47D, MCF7 and MDA-MB231 cells lacking STARD7 (Fig. 2F). Of note, the ER stress inducer RNA-dependent protein kinase (PKR)-like ER kinase (PERK), which is enriched in MAMs [31], was found elevated upon STARD7

deficiency in all tested breast cancer cell lines, especially in MDA-MB231 cells (Fig. 2F). Levels of other ER stress downstream targets such as Eukaryotic Initiation Factor 2α (EIF2α), X box-binding protein 1 (XBP1) and Activating transcription factor 4 (ATF4) were robustly elevated upon STARD7 deficiency in MDA-MB231 but not in both T47D and MCF7 cells, as were BIP levels (Fig. 2F). Levels of the lysosomal protein LAMP1 were increased upon STARD7 deficiency in MAMs as well as in mitochondrial extracts (Fig. 2E). Importantly, levels of RAB11, which is associated with recycling endosomes, were decreased upon STARD7 deficiency in both MAMs and mitochondrial extracts, suggesting that the recycling of some key membrane receptors such as EGFR may be impaired in cells lacking STARD7 (Fig. 2E). Therefore, STARD7 deficiency alters protein levels of many but not all proteins in MAMs.

# Loss of STARD7 leads to a metabolic and epigenetic-mediated transcriptional reprogramming

To address consequences of STARD7 deficiency on mitochondrial functions, we performed LC-MS metabolomics and established the metabolic signature of both control and STARD7-depleted cells (Figs. 3A and 3B). An enrichment overview of these signatures revealed numerous deregulated metabolic pathways in breast cancer cells lacking STARD7 (Fig. 3A). Fatty acids (FA) β-oxidation was severely upregulated in breast cancer cell lacking STARD7 (Fig. 3A). Of note, levels of Acetyl-CoA carboxylase (ACC), which catalyzes the carboxylation of acetyl-CoA into malonyl-CoA [32], were downregulated upon STARD7 deficiency in both MCF7 and T47D cells (Fig. 3C). As a consequence, its phosphorylated and inactivated form (pACC) was also downregulated upon STARD7 deficiency (Fig. 3C). Interestingly, acetyl-carnitine, which is synthesized from acetyl-CoA by Carnitine palmitoyltransferase I (CPTI), the key limiting-step of FA β-oxidation [33], accumulated in MCF7 cells lacking STARD7 (Fig. 3B). Likewise, STARD7 deficiency led to enhanced levels of a variety of Carnitine derivatives, suggesting that mitochondrial capacity to oxidize FAs may be overwhelmed in these cells, which causes accumulation of toxic lipid intermediates (Fig. 3B) [34]. Importantly, levels of the universal methyl donor for methylation reactions S-Adenosyl-L-methionine (SAM) were also elevated in MCF7 cells lacking STARD7 (Figs. 3B and 3D). Such observation was also seen upon STARD7 deficiency in MDA-MB231 cells (Fig. 3D). As a result, the methylation potential of both cell lines was increased upon STARD7 deficiency (Fig. 3D). In contrast, steady state levels of both creatine and phosphocreatine were significantly reduced upon STARD7 deficiency (Fig. 3B). Therefore, a severe metabolic reprogramming occurs in breast cancer cells lacking STARD7.

As STARD7 deficiency causes the accumulation of SAMs in breast cancer cells and given its role in epigenetic modifications through both histone and DNA methylations, we next conducted ChIP Sequencing experiments using the anti-H3K27Me3 antibody to establish the methylome of both control and STARD7-depleted MCF7 cells. Histone H3 trimethylation on histone 27 is associated with transcriptional repression and is catalyzed by the methyltransferases EZH1 and EZH2 [35,36]. The frequency of H3K27Me3 events increased in cells lacking STARD7 (Fig. 3E). This epigenetic modifications was found in promoters as well as in the first or other exons and introns and in 3’ and 5’ UTRs and this distribution did not change upon STARD7 deficiency (Fig. 3F). Interestingly, H3K27Me3

events were enriched on specific gene candidates linked to cell proliferation, cell cycle and oxidative stress (Fig. 3G). In this context, the H3K27Me3 epigenetic mark was found elevated on the promoter of both NUF2, a member of the kinetochore complex [37] and Thioredoxin-interacting protein (TXNIP), an Thioredoxin inhibitor [38] (Fig. 3G). As a result, TXNIP protein levels were downregulated in breast cancer cells lacking STARD7 (Fig. 3H). Moreover, levels of Thioredoxin reductase (TRXR1), which plays a key role in protection against oxidant injury [39], were increased in breast cancer cells lacking STARD7 (Fig. 3H). Therefore, the accumulation of SAMs seen upon STARD7 deficiency has dramatic consequences on the transcription of specific candidates involved in cell proliferation and in the response to oxidative stress.

# Loss of STARD7 leads to cell cycle arrest in breast cancer cells

To learn more on gene candidates whose expression is regulated by STARD7, we next established the transcriptomic signature of control versus STARD7-depleted breast cancer cells by RNA Sequencing experiments. STARD7 deficiency had dramatic consequences on the transcriptomic signature as hundreds of candidates were not properly expressed (Fig. 4A). Interestingly, many dysregulated candidates were functionally linked to DNA metabolic processes, mitotic cell cycle phase transition and DNA replication (Fig. 4B). A HeatMap illustrating the most 30 downregulated genes upon STARD7 deficiency in MCF7 cells included key actors of cell progression such as Cyclin D1 (CCND1), IGFBP4, MYB and MYBL1 (Fig. 4C). Gene Set Enrichment Analyses (GSEA) conducted with RNA Sequencing data confirmed that STARD7 deficiency was linked to defects in the G2M checkpoint and in the expression of c-MYC targets, suggesting a role for STARD7 in cell cycle progression (Fig. 4D). Real-Time PCR analyses carried out with total RNAs from both control and STARD7-depleted MCF7 or T47D cells confirmed that Polo-like kinase 1 (PLK1), c-MYC, estrogen receptor 1 (ESR1, here after referred to as ERα), retinoic acid receptor alpha (RARA), Carbonic Anhydrase 12 (CA12), IGFBP4, Cyclin D1, Cyclin B1 (CCNB1) mRNA levels were decreased (Figs. 4E and S1, respectively). Consistently, a variety of Cyclins were not properly expressed at the protein level in MCF7 cells lacking STARD7 (Fig. 4F). Indeed, STARD7 deficiency impaired the expression of Cyclin A, B1 and B2 in MCF7 cells but also in the triple negative breast cancer-derived MDA-MB-231 cell line (Fig. 4F). On the other hand, cyclin kinase inhibitors such as p21 and p27 levels were enhanced upon STARD7 deficiency (Fig. 4F). Therefore, STARD7 deficiency triggers a transcriptional reprogramming linked to cell cycle arrest.

# STARD7 deficiency impairs signaling pathways linked to cell proliferation in breast cancer cells

Because STARD7 deficiency impairs ERα mRNA levels in MCF7 cells, we next assessed whether ERα signaling was defective in these cells. MCF7 cells lacking STARD7 showed lower protein levels of ERα while levels of SOX9 were elevated (Fig. 5A). Consistently, ERα signaling was severely defective in STARD7-depleted T47D cells, as evidenced by a defective estrogen (E2)-dependent ERα phosphorylation,

at least due to severely decreased ERα protein levels (Fig. 5B). As a result, the estrogens-dependent induction of c-Myc, Cyclins A, B2 and D1 was severely impaired in T47D cells lacking STARD7 (Fig. 5B). Here again, T47D cells lacking STARD7 showed elevated levels of both p21 and p27 (Fig. 5B). Consistently, mRNA levels of growth regulation by estrogen in breast cancer 1 (GREB1), an early-response gene in the estrogen receptor-regulated pathway that promotes hormone-dependent cell proliferation [40], were not properly induced by estrogens in T47D cells lacking STARD7 (Fig. 5C). Likewise, estrogens fails to trigger cell cycle progression in T47D cells lacking STARD7, as evidenced by FACS analyses (Fig. 5D). Therefore, STARD7 is involved in ERα signaling, at least by promoting ERα expression.

As ERα$^+$ cells lacking STARD7 showed cell proliferation defects, we also looked at levels of growth factor receptors and found that STARD7 was dispensable for both HER2 and HER3 expression in MCF7 cells (Fig. 6A). Moreover, STARD7 deficiency modestly impaired EGFR levels (Fig. 6A). TNBC-derived MDA-MB-231 cells also showed defects upon STARD7 deficiency but molecular mechanisms where different when compared to MCF7 cells as both EGFR and HER2 but not HER3 were not properly expressed in these TNBC-derived cells (Fig. 6B). Moreover and in contrast to MCF7 cells lacking STARD7, MDA-MB-231 cells showed lower levels of SOX9 upon STARD7 deficiency (Fig. 6B). Consistently, EGF-dependent EGFR phosphorylation on Tyrosine 1068 was severely impaired in MDA-MB-231 cells lacking STARD7 (Fig. 6C). Therefore, STARD7 is essential for EGFR signaling in TNBC-derived cells, at least by promoting EGFR expression. To better understand why EGFR protein levels decreases in TNBC cells lacking STARD7, we assessed EGF-dependent EGFR degradation in these cells. To prevent EGFR neosynthesis, we first pre-treated control and STARD7-depleted cells with Cycloheximide, a translation inhibitor and subsequently followed EGFR levels upon EGF stimulation. As expected, EGFR protein levels decreased upon EGF stimulation both in control and STARD7-depleted cells (Fig. 6D, left panel). Moreover, the proteasome inhibitor MG132 did not restore EGFR levels in cells lacking STARD7, suggesting that EGFR-dependent degradation does not rely on the proteasome in these cells (Fig. 6D, middle panel). As expected, the lysosome inhibitor BaFA1 blocked EGF-dependent EGFR degradation in control cells (Fig. 6D, right panel). Importantly, BafA1 also restored EGFR levels in cell lacking STARD7 and also decreased EGF-dependent EGFR degradation when compared to STARD7-depleted cells treated with EGF and DMSO (Fig. 6D). Collectively, these results suggest that TNBC cells lacking STARD7 show enhanced Lysosome-dependent EGFR degradation. To further support this conclusion, we also assessed EGF-bound EGFR trafficking in control versus STARD7-depleted MDA-MB231 cells. EGF-bound EGFR was found in EEA1$^+$ endosomes 30 minutes post-EGF stimulation in both control and STARD7-depleted MDA-MB231 cells (Fig. 6E). Importantly, we found an increase of enlarged EEA1$^+$ endosomes in cells lacking STARD7 (Fig. 6E). Moreover, electronic microscopy analyses indicated that cells lacking STARD7 also showed less endosomes with tubular structures known to be involved in membrane receptor recycling (Fig. 6F). Indeed, while 10 out of 30 control cells showed at least one endosome with tubular structures, only 5 out of 31 cells lacking STARD7 did (Fig. 6F). Collectively, these results indicate that STARD7 controls the size of early endosomes and promotes membrane receptor recycling.

# STARD7 deficiency impairs the expression of candidates involved in DNA replication

To further confirm the link between STARD7 and cell cycle progression, we established the proteomic signature of both control and STARD7-depleted MCF7 cells and found again that DNA replication was the main biological process controlled by STARD7 in breast cancer cells (Fig. S2A). Indeed, key biological processes involving downregulated candidates upon STARD7 deficiency were cell DNA replication and DNA metabolic process (Fig. S2B). In agreement with our western blot analyses, Cyclin D1 and c-Myc were identified as downregulated candidates in MCF7 cells lacking STARD7 (Fig. 7A). Here again, a String Interaction Network analyses highlighted a link between STARD7 expression and DNA replication (Fig. 7B). Likewise, levels of candidates involved in kinetochore formation were downregulated in cells lacking STARD7 (Fig. 7C). Indeed, levels of NUF2, a core component of the kinetochore outer plate, were decreased upon STARD7 deficiency, most likely due to the enhanced distribution of the H3K27Me3 epigenetic mark on NUF2 promoter (Figs. 7C and 3G, respectively). Moreover, NDC80, a NUF2-associated protein [37], was also less expressed in cells lacking STARD7 (Fig. 7C). Other members of the kinetochore such as CENPE as well as Kinesins such as KIF15 and KIF4B were also downregulated upon STARD7 deficiency in breast cancer cells (Fig. 7C). Therefore, STARD7 supports DNA replication, at least by promoting kinetochore assembly in breast cancer cells.

# STARD7 deficiency potentiates a ciliogenesis signature in breast cancer cells

To learn more on biological processes regulated by STARD7, we concentrated on candidates upregulated in MCF7 cells lacking STARD7 and found that multiple candidates were involved in intraciliary transport, cilium assembly and organization (Figs. 8A to 8C). Real-Time PCR analyses indeed confirmed that WDR19, DNAH1, DNAAF4, IFT22/43 and CFAP69 were more strongly expressed in STARD7-depleted T47D cells, while levels of PLA2G3, a negative regulator of ciliogenesis were up (Fig. 8D). Likewise, STARD7 deficiency in the human retinal pigment epithelial RPE-1 cell line immortalized with hTERT (« hTERT-RPE1 » cells), an experimental model to assess ciliogenesis, enhances the length of the primary cilium, as evidenced by anti-Arl13b immunofluorescent analyses (Fig. 8E). Therefore, STARD7 is a negative regulator of ciliogenesis.

# Loss of STARD7 leads to autophagy

Because autophagy promotes primary ciliogenesis, we next explored whether breast cancer cells lacking STARD7 undergo autophagy [41]. We first noticed that multiple lysosomal proteins such as Niemann-Pick C2 protein (NPC2), N-acetyl-alpha-glucosaminidase (NAGLU) and Lysosomal-associated membrane protein 1 (LAMP1) were enriched at the mRNA level in breast cancer cells lacking STARD7 (Fig. 9A). Likewise, MCF7, T47D and MDA-MB231 cells lacking STARD7 showed elevated levels of the conjugated form of LC3B (LC3BII), a sign of autophagy (Fig. 9B, top panels). Consistently, the LC3BII/LC3BI ratio was elevated in all breast cancer cell lines treated with Chloroquine (Fig. 9B, bottom panels). Breast cancer

cells lacking STARD7 also showed elevated levels of LAMP1 or LAMP2, which, together with FACS analyses using Lysotracker, demonstrates that STARD7 deficiency leads to an increased in lysosomal biomass, a hallmark of autophagy (Fig. 9C). Likewise, STARD7-depleted MCF7 cells showed a more pronounced colocalization of LC3B with p62 or with LAMP1, as judged by immunofluorescence analyses (Figs. 9D and S4, respectively).

To prove that the ciliogenesis signature seen upon STARD7 deficiency in breast cancer cells results from autophagy, we next quantified mRNA levels of candidates involved in ciliogenesis in MCF7 cells treated with the mTORC1 inhibitor Rapamycin. In circumstances in which autophagy is triggered by Rapamycin, mRNA levels of multiple candidates dramatically increased (Fig. 9E). We also treated MCF7 cells with Chloroquine, which inhibits autophagy by blocking autophagosome fusion with lysosomes. Chloroquine severely decreased DNAAF4 and IFT22 mRNA levels and did not significantly changed DNAH1, CFAF69 and WDR19 mRNA levels. Interestingly, levels of PLA2G3, a negative regulator of ciliogenesis [42], were downregulated upon Rapamycin treatment, suggesting that this candidate is regulated by mTORC1 (Fig. 9E). Collectively, these data indicate that ciliogenesis occurs in breast cancer cells undergoing autophagy.

# DISCUSSION

We provide here insights into molecular mechanisms through which metabolic reprogramming influence gene transcription with important consequences on cell cycle. The loss of the lipid transfer protein STARD7 leads to SAM accumulation, which causes a transcriptional repression due to the accumulation of H3K27me3 on genes involved in cell proliferation. Moreover, breast cancer cells lacking STARD7 do not properly signal through both ERα and EGFR and also show signs of autophagy and ciliogenesis. Therefore, our data demonstrate that breast cancer cells of any subtype ($ERα^+$ tumors and TNBCs) overexpress STARD7 to support cell proliferation.

Breast cancer cells lacking STARD7 show a profound modification of mitochondrial ultrastructure. Indeed, their mitochondria are all in the orthodox state showing a more expanded matrix in which FA oxidation occurs. This observation fits with the fact that STARD7-depleted cells accumulate Carnitine derivatives, which is indicative of increased FA oxidation. Accumulation of Carnitine derivatives may reflect overwhelmed mitochondria, a process ultimately leading to lipotoxicity. Molecular mechanisms underlying enhanced FA oxidation upon STARD7 deficiency is currently unclear. Carnitine palmitoyltransferases, which shuttle acylcarnitines between mitochondrial membranes, are properly expressed in breast cancer cells lacking STARD7 (data not shown). It is worth mentioning that levels of ACC, which produces malonyl-CoA, an inhibitor of FA oxidation [43], are downregulated in breast cancer cells lacking STARD7. Therefore, this finding may explain why STARD7 deficiency is linked to enhanced FA oxidation.

Accumulation of SAMs is an important feature of STARD7-depleted breast cancer cells. Our data demonstrate that enhanced SAM levels impact on gene transcription through the deposition of the

H3K27me3 epigenetic mark on candidates involved in cell cycle progression. Yet, multiple candidates downregulated upon STARD7 deficiency do not show differences of histone methylation on their promoter. Indeed, our transcriptomic and ChiP Sequencing data do not significantly overlap, indicating that additional mechanisms underly the capacity of STARD7 to promote cell cycle progression. Additional mechanisms may include UPR signaling, as multiple UPR effectors such as PERK, BIP and XBP1 are more expressed in TNBC-derived cells lacking STARD7. Importantly, we found that EGFR was massively downregulated in TNBC-derived cells lacking STARD7, a phenomenon that cannot be explained by the SAM-dependent epigenetic-mediated silencing. Cells lacking STARD7 actually show less endosomes with tubular structures, which, combined with decreased Rab11 levels, suggests that EGFR recycling is impaired. Consistently, EGFR degradation through lysosomes is potentiated upon STARD7 deficiency, indicating that the loss of a lipid transfer protein has dramatic consequences on the trafficking of membrane receptors, at least through deregulated contacts between several intracellular organels. ERα is another candidate not found in our ChIP Sequencing data, despite a massively downregulated expression upon STARD7 deficiency in MCF7 cells but the underlying molecular mechanisms remain unclear.

It is currently unknown why breast cancer cells lacking STARD7 accumulate SAMs. One reason may come from the role of STARD7 in Coenzyme Q synthesis [9]. Coenzyme synthesis, a multi-step process, requires SAM as a co-factor for both *O*- and *C*2-methylations [44]. Therefore, SAMs accumulation may be an indirect consequence of a defective Coenzyme Q synthesis seen in breast cancer lacking STARD7. Interestingly, we also noticed that STARD7 deficiency downregulated creatine levels, possibly because of a defective synthesis. If so, it is important to mention that creatine synthesis also relies on the methyl donor SAM, similarly to Coenzyme synthesis [45]. Here again, a defective creatine synthesis may contribute to elevated SAM levels seen in breast cancer cells lacking STARD7.

It was first demonstrated that STARD7 deficiency causes defects in PC transport to mitochondria. It is therefore not surprising to see that STARD7 deficiency deregulates multiple metabolic pathways occurring in this organelle. The enhanced mitochondria-ER contact sites seen in breast cancer cells lacking STARD7 may be a compensatory mechanism to support lipid transfer. Yet, MAMs are essential for the ER-mitochondria $Ca^{2+}$ transfer but more mitochondria-ER contact sites seen upon STARD7 deficiency may lead to mitochondrial $Ca^{2+}$ overload, which triggers apoptosis. Interestingly, levels of the voltage-dependent anion channel VDAC are dramatically decreased in MAMs and this could be seen as a pro-survival adaptation in breast cancer cells lacking STARD7.

As an evidence linking the phenotype of STARD7-depleted breast cancer cells with a mitochondrial function of STARD7, interactomic studies carried out with mitochondrial proteins identified an interaction between STARD7 and several candidates, including CHCD10 [46]. Interestingly, CHCHD10 protein levels were severely downregulated in breast cancer cells lacking STARD7, as demonstrated through our proteomic studies, suggesting that STARD7 binds and stabilizes CHCHD10. Therefore, phenotypic

alterations found in breast cancer cells lacking STARD7 result from multiple molecular mechanisms, including a defective PC transport and CHCHD10 protein destabilization.

In conclusion, our study define STARD7 as a candidate that promotes cell proliferation in breast cancer, at least through ERα and EGFR signaling. It remains to be seen whether STARD7 inhibition would be an elegant pharmacological approach to treat breast malignancies and/or to overcome resistance to targeted therapies through the induction of cell death.

## Declarations

# AUTHOR CONTRIBUTIONS

Conceptualization, E.D. and A.C.; Methodology, E.D., C.M., P.A-F., A.B., A.L., L.K., M.T., I.N., R.K., J.M Jr., A.von K., N.H., K.S. and A.C; Validation, E.D., A.L., M.T., I.N., A.von K., N.H. and A.C; Formal Analysis, E.D., A.L., M.T., I.N., A.von K., N.H., K.S. and A.C. Investigation, E.D., C.M., P.A-F., A.B., A.L., L.K., M.T., I.N., R.K., J.M Jr., A.von K., K.S. and A.C., Resources, A.B., P.C., G.P. Writing-Original Draft, A.C. Writing-Review & Editing, E.D., K.S. and A.C. Visualization, E.D., K.S. and A.C. Supervision, A.C. Project Administration and Funding Acquisition, A.C.

# ACKNOWLEDGMENTS

The authors are grateful to the GIGA Imaging platform for the IF analyses. This work was supported by grants from WELBIO (WELBIO-CR-2019C-02R), FNRS/TELEVIE, the Belgian Foundation against Cancer (FBC/2020/1323), the University of Liege (ARC UBICOREAR) and by the Leon Fredericq Foundation (Faculty of Medicine, CHU of Liege). PC and AC are Senior Research Associate and Research Director at the FNRS, respectively. The authors do not declare any conflict of interest.

## References

1. Scharwey M, Tatsuta T, Langer T. Mitochondrial lipid transport at a glance. *Journal of Cell Science* 2013; **126**: 5317–5323.
2. Tarasov A, Griffiths E, Rutter G. Regulation of ATP production by mitochondrial Ca2+. *Cell Calcium* 2012; **52**: 28–35.
3. Willems P, Rossignol R, Dieteren C, Murphy M, Koopman W. Redox Homeostasis and Mitochondrial Dynamics. *Cell Metabolism* 2015; **22**: 207–218.
4. Durand S, Angeletti S, Genti-Raimondi S. GTT1/StarD7, a novel phosphatidylcholine transfer protein-like highly expressed in gestational trophoblastic tumour: cloning and characterization. *Placenta* 2004; **25**: 37–44.
5. Horibata Y, Ando H, Zhang P, Vergnes L, Aoyama C, Itoh M *et al.* StarD7 mediates the intracellular trafficking of phosphatidylcholine to mitochondria. *The Journal of biological chemistry* 2010; **285**:

7358–7365.

6. Horibata Y, Ando H, Zhang P, Vergnes L, Aoyama C, Itoh M *et al.* StarD7 Protein Deficiency Adversely Affects the Phosphatidylcholine Composition, Respiratory Activity, and Cristae Structure of Mitochondria. *The Journal of biological chemistry* 2016; **291**: 24880–24891.
7. Yang L, Na C, Luo S, Wu D, Hogen S, Huang T *et al.* The Phosphatidylcholine Transfer Protein Stard7 is Required for Mitochondrial and Epithelial Cell Homeostasis. *Nature Scientific Reports* 2017; **7**: 46416.
8. Saita S, Tatsuta T, Lampe P, König T, Ohba Y, Langer T. PARL partitions the lipid transfer protein STARD7 between the cytosol and mitochondria. *EMBO Journal* 2018; **37**: e97909.
9. Deshwal S, Onishi M, Tatsuta T, Bartsch T, Cors E, Ried K *et al.* Mitochondria regulate intracellular coenzyme Q transport and ferroptotic resistance via STARD7. *Nature Cell Biology* 2023; **25**: 246–257.
10. Conde de la Rosa L, Garcia-Ruiz C, Vallejo C, Baulies A, Nunez S, Monte M *et al.* STARD1 promotes NASH-driven HCC by sustaining the generation of bile acids through the alternative mitochondrial pathway. *Journal of Hepatology* 2021; **74**: 1429–1441.
11. Akiyama N, Sasaki H, Ishizuka T, Kishi T, Sakamoto H, Onda M *et al.* Isolation of a candidate gene, CAB1, for cholesterol transport to mitochondria from the c-ERBB-2 amplicon by a modified cDNA selection method. *Cancer Research* 1997; **57**: 3548–3553.
12. Vassilev B, Sihto H, Li S, Hölttä-Vuori M, Ilola J, Lundin J *et al.* Elevated levels of StAR-related lipid transfer protein 3 alter cholesterol balance and adhesiveness of breast cancer cells: potential mechanisms contributing to progression of HER2-positive breast cancers. *American Journal of Pathology* 2015; **185**: 987–1000.
13. Li P, Zhang Z, Lv H, Sun P. Inhibiting the expression of STARD3 induced apoptosis via the inactivation of PI3K/AKT/mTOR pathway on ER+ breast cancer. *Tissue and Cell* 2022; **79**: 101971.
14. Zhang M, Xiang Z, Wang F, Shan R, Li L, Chen J *et al.* STARD4 promotes breast cancer cell malignancy. *Oncology Reports* 2020; **44**: 2487–2502.
15. Olayioye M, Hoffmann P, Pomorski T, Armes J, Simpson R, Kemp B *et al.* The phosphoprotein StarD10 is overexpressed in breast cancer and cooperates with ErbB receptors in cellular transformation. *Cancer Research* 2004; **64**: 3538–3544.
16. Floris A, Luo J, Frank J, Zhou J, Orrù S, Biancoletta M *et al.* Star-related lipid transfer protein 10 (STARD10): a novel key player in alcohol-induced breast cancer progression. *Journal of Experimental & Clinical Cancer Research* 2019; **38**: 4.
17. Ewels PA, Peltzer A, Fillinger S, Patel H, Alneberg J, Wilm A *et al.* The nf-core framework for community-curated bioinformatics pipelines. Nature Biotechnology. 2020; **38**: 276–278.
18. Wieckowski M, Giorgi C, Lebiedzinska M, Duszynski J, Pinton P. Isolation of mitochondria-associated membranes and mitochondria from animal tissues and cells. *Nature Protocols* 2009; **4**: 1582–1590.
19. Li H, Handsaker B, Wysoker A, Fennell T, Ruan J, Homer N *et al.* The Sequence Alignment/Map format and SAMtools. *Bioinformatics* 2009; **25**: 2078–2079.

20. Langmead B, Salzberg S. Fast gapped-read alignment with Bowtie 2. 2012; **9**: 357–359.
21. Ramirez F, Ryan D, Grüning B, Bhardwaj V, Kilpert F, Richter A *et al.* deepTools2: a next generation web server for deep-sequencing data analysis. *Nucleic Acids Research* 2016; **44**: W160-165.
22. Zhang Y, Liu T, Meyer C, Eeckhoute J, Johnson D, Bernstein B *et al.* Model-based analysis of ChIP-Seq (MACS). *Genome Biology* 2008; **9**: R137.
23. Yu G, Wang L, He Q. ChIPseeker: an R/Bioconductor package for ChIP peak annotation, comparison and visualization. *Bioinformatics* 2015; **31**: 2382–2383.
24. Yu C, Wang L, Han Y, He Q. clusterProfiler: an R package for comparing biological themes among gene clusters. *OMICS* 2012; **16**: 284–287.
25. Filadi R, Pendin D, Pizzo P. Mitofusin 2: from functions to disease. *Cell Death & Diseases* 2018; **9**: 330.
26. Smirnova E, Griparic L, Shurland D-L, van der Bliek A. Dynamin-related Protein Drp1 Is Required for Mitochondrial Division in Mammalian Cells. *Molecular Biology of the Cell* 2001; **12**: 2245–2256.
27. Ihenacho U, Meacham K, Harwig M, Widlansky M, Hill R. Mitochondrial Fission Protein 1: Emerging Roles in Organellar Form and Function in Health and Disease. *Frontiers in Endocrinology* 2021; **12**.
28. Yu H, Sun C, Gong Q, Feng D. Mitochondria-Associated Endoplasmic Reticulum Membranes in Breast Cancer. *Frontiers in cell and developmental biology* 2021; **9**: 629669.
29. Sassano M, van Vliet A, Agostinis P. Mitochondria-Associated Membranes As Networking Platforms and Regulators of Cancer Cell Fate. *Frontiers in Oncology* 2017; **7**: 174.
30. Carreras-Sureda A, Jana F, Urra H, Durand S, Mortenson D, Sagredo A *et al.* Non-canonical function of IRE1α determines mitochondria-associated endoplasmic reticulum composition to control calcium transfer and bioenergetic. *Nature Cell Biology* 2019; **21**: 755–767.
31. Verfaillie T, Rubio N, Garg A, Bultynck G, Rizzuto R, Decuypere J-P *et al.* PERK is required at the ER-mitochondrial contact sites to convey apoptosis after ROS-based ER stress. *Cell Death and Differentiation* 2012; **19**: 1880–1891.
32. Tong L. Acetyl-coenzyme A carboxylase: crucial metabolic enzyme and attractive target for drug discovery. *Cellular and Molecular Life Sciences* 2005; **62**: 1784–1803.
33. Qu Q, Zeng F, Liu X, Wang Q, Deng F. Fatty acid oxidation and carnitine palmitoyltransferase I: emerging therapeutic targets in cancer. *Cell Death & Diseases* 2016; **7**: e2226.
34. Jaishy B, Abel E. Lipids, lysosomes, and autophagy. *Journal of Lipid Research* 2016; **57**: 1619–1635.
35. Kuzmichev A, Nishioka K, Erdjument-Bromage H, Tempst P, Reinberg D. Histone methyltransferase activity associated with a human multiprotein complex containing the Enhancer of Zeste protein. *Genes and Development* 2002; **16**: 2893–2905.
36. Boyer L, Plath K, Zeitlinger J, Brambrink T, Medeiros L, Lee T *et al.* Polycomb complexes repress developmental regulators in murine embryonic stem cells. *Nature* 2006; **441**: 349–353.
37. Liu D, Ding X, Du J, Cai X, Huang Y, Ward T *et al.* Human NUF2 interacts with centromere-associated protein E and is essential for a stable spindle microtubule-kinetochore attachment. *Journal of*

*Biological Chemistry* 2007; **282**: 21415–21424.

38. Nishiyama A, Matsui M, Iwata S, Hirota K, Masutani H, Nakamura H *et al.* Identification of thioredoxin-binding protein-2/vitamin D(3) up-regulated protein 1 as a negative regulator of thioredoxin function and expression. *Journal of Biological Chemistry* 1999; **274**: 21645–21650.
39. Mustacich D, Powis G. Thioredoxin reductase. *Biochemical Journal* 2000; **346**: 1–8.
40. Rae JM, Johnson MD, Scheys JO, Cordero KE, Larios JM, Lippman ME. GREB1 is a critical regulator of hormone dependent breast cancer growth. *Breast Cancer Research and Treatment* 2005; **92**: 141–149.
41. Tang Z, MG L, Stowe T, Chen S, Zhu M, Stearns T *et al.* Autophagy promotes primary ciliogenesis by removing OFD1 from centriolar satellites. *Nature* 2013; **502**: 254–257.
42. Kim J, Lee J, Heynen-Genel S, Suyama E, Ono K, Ideker T *et al.* Functional genomic screen for modulators of ciliogenesis and cilium length. *Nature* 2010; **464**: 1048–1051.
43. Foster D. Malonyl-CoA: the regulator of fatty acid synthesis and oxidation. *Journal of Clinical Investigation* 2012; **122**: 1958–1959.
44. Stefely J, Pagliarini D. Biochemistry of Mitochondrial Coenzyme Q Biosynthesis. *Trends in Biochemical Sciences* 2017; **42**: 824–843.
45. Stead L, Brosnan J, Brosnan M, Vance D, Jacobs R. Is it time to reevaluate methyl balance in humans? *American Journal of Clinical Nutrition* 2006; **83**: 8–10.
46. Floyd B, Wilkerson E, Veling M, Minogue C, Xia C, Beebe E *et al.* Mitochondrial Protein Interaction Mapping Identifies Regulators of Respiratory Chain Function. *Molecular Cell* 2016; **4**: 621–632.

# Figures

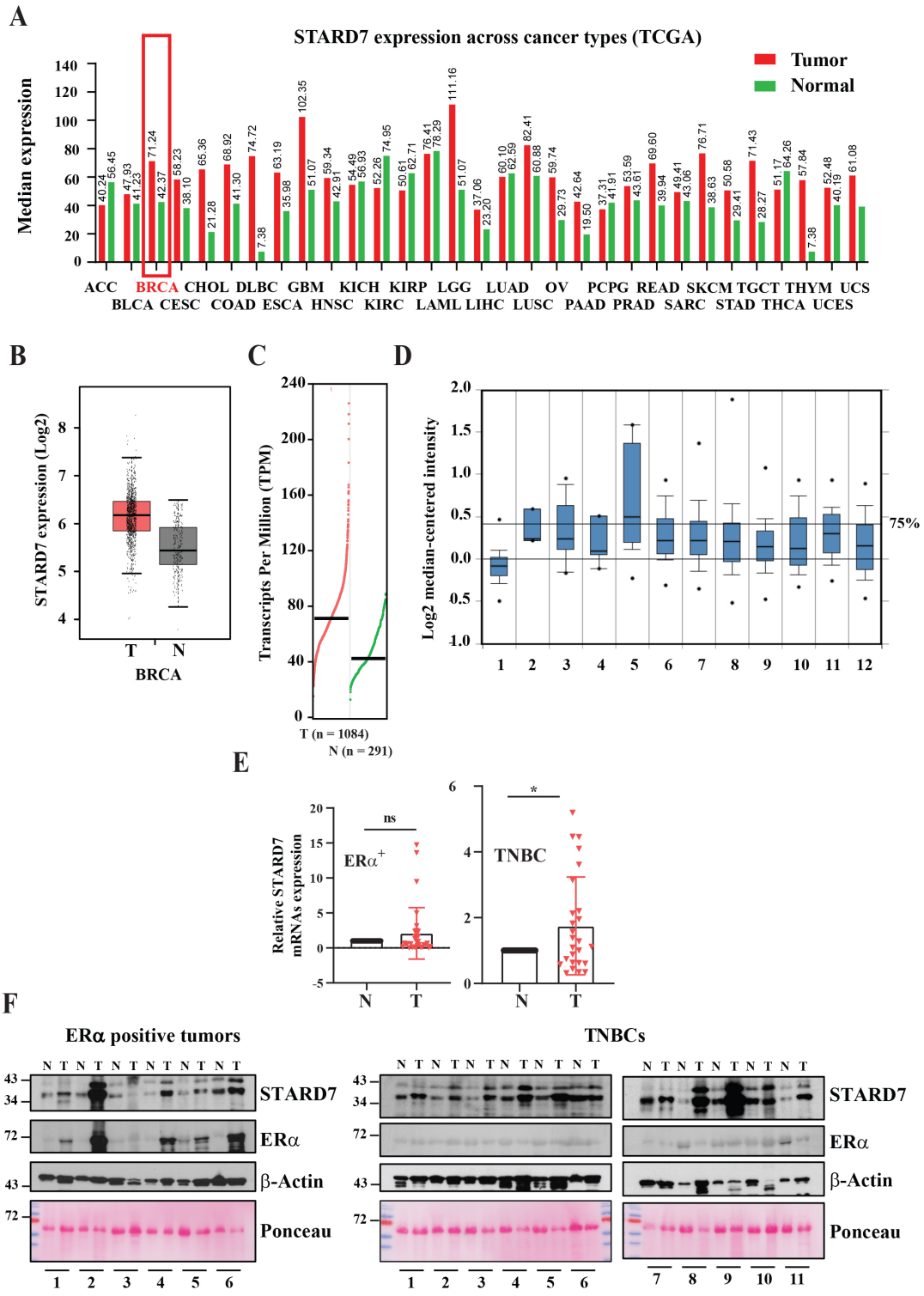


*Figure 1*

## Figure 1

**STARD7 overexpression in breast cancer. A.** STARD7 expression in multiple human cancer types. TCGA data with mRNA expression levels of STARD7 in human cancer types are illustrated. **B.** and **C.** Enrichment of STARD7 mRNAs in breast cancer versus normal adjacent tissues (TCGA data). **D.** STARD7 overexpression in human breast cancer. STARD7 mRNA levels were quantified in the following cases : 1. Breast (144), 2. Benign Breast Neoplasm (3), 3. Breast Carcinoma (14), 4. Breast Phyllodes Tumor (5), 5.

Ductal Breast Carcinoma in Situ (10), 6. Invasive Breast Carcinoma (21), 7. Invasive Ductal and Invasive Lobular Breast Carcinoma (90), 8. Invasive Ductal Breast Carcinoma (1,556), 9. Invasive Lobular Breast Carcinoma (148), 10. Medullary Breast Carcinoma (32), 11. Mucinous Breast Carcinoma (46) and 12. Tubular Breast Carcinoma (67). **E.** Enhanced STARD7 mRNA levels in TNBCs but not in $ER^+$ breast cancers. Real-Time PCRs were conducted with total RNAs extracted from clinical cases of breast cancer ("T") as well as from corresponding normal adjacent tissues ("N"). mRNA levels in normal adjacent tissues were set to 1 and levels in tumors were relative to that after normalization with GAPDH levels (mean +/- SD, Student T-test, * = $p < 0.05$). **F.** Enhanced STARD7 protein levels in human breast cancer. Extracts from $ER^+$ and TNBCs as well as from corresponding adjacent normal tissues were subjected to western blot analyses using the indicated antibodies.

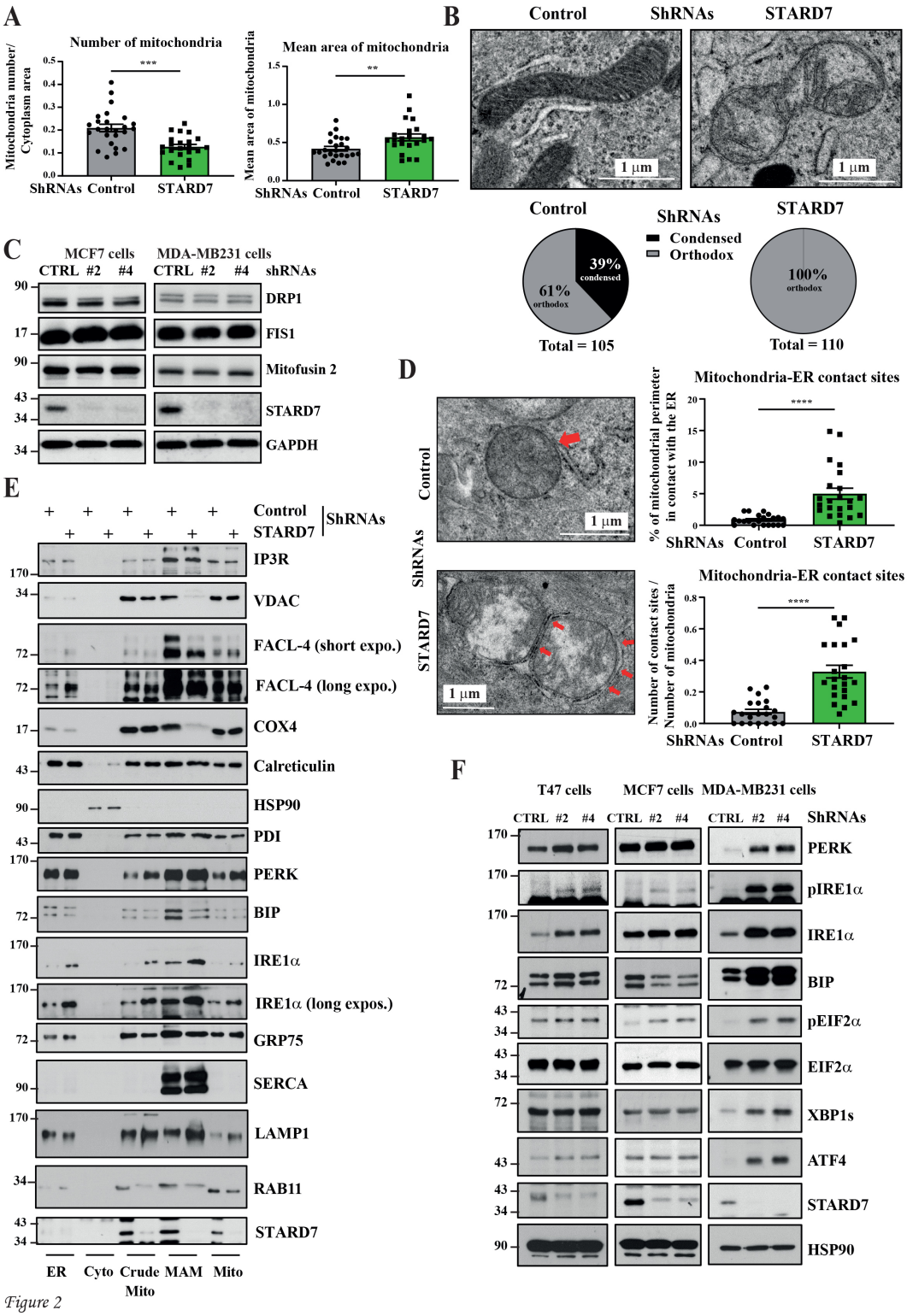


*Figure 2*

## Figure 2

**STARD7 deficiency leads to changes in mitochondrial morphology in breast cancer cells. A.** Enhanced number and size of mitochondria upon STARD7 deficiency. A quantitative analysis of mitochondria observed by Transmission Electron Microscopy (TEM) in control and STARD7-depleted breast cancer cells is illustrated. The average number of mitochondria by cytoplasmic area and the average area of mitochondria are shown (top and bottom histograms, respectively) (*** = $p < 0.001$). **B.**Accumulation of

mitochondria in the orthodox state upon STARD7 deficiency. On the top, the ultrastructure of mitochondria in control and STARD7-depleted breast cancer cells is illustrated. At the bottom, the percentage of mitochondria in orthodox or condensed state is mentioned in control and STARD7-depleted breast cancer cells (see methods for details). **C.** STARD7 is dispensable in mitochondria dynamics. Extracts from control and STARD7-depleted MCF7 and MDA-MB231 cells were subjected to western blot analyses using the indicated antibodies. **D.** Enhanced mitochondria-ER contact sites in breast cancer cells lacking STARD7. TEM analysis of mitochondria/ER contacts in control and STARD7-depleted MCF7 cells. On the left, illustration of the ultrastructure of mitochondria/ER contacts in both control and STARD7-depleted MCF7 cells. On the right, number of mitochondria/ER contact sites and average percentage of mitochondrial perimeter in contact with the ER are plotted (top and bottom histograms, respectively). **E.**Enrichment of some but not all MAMs markers in MAMs upon STARD7 deficiency. Extracts from MCF7 cells were biochemically fractionated to generate organelle-enriched extracts. ER = endoplasmic reticulum, Cyto = cytoplasm, Crude mito = crude mitochondria, MAM = mitochondria-associated membrane, Mito = mitochondria. The organelle-enriched extracts were subjected to western blots using the indicated antibodies. **F.**Elevated levels of MAMs markers in breast cancer cell lacking STARD7. Extracts from control and STARD7-depleted MCF7 cells were subjected to western blot analyses using the indicated antibodies.

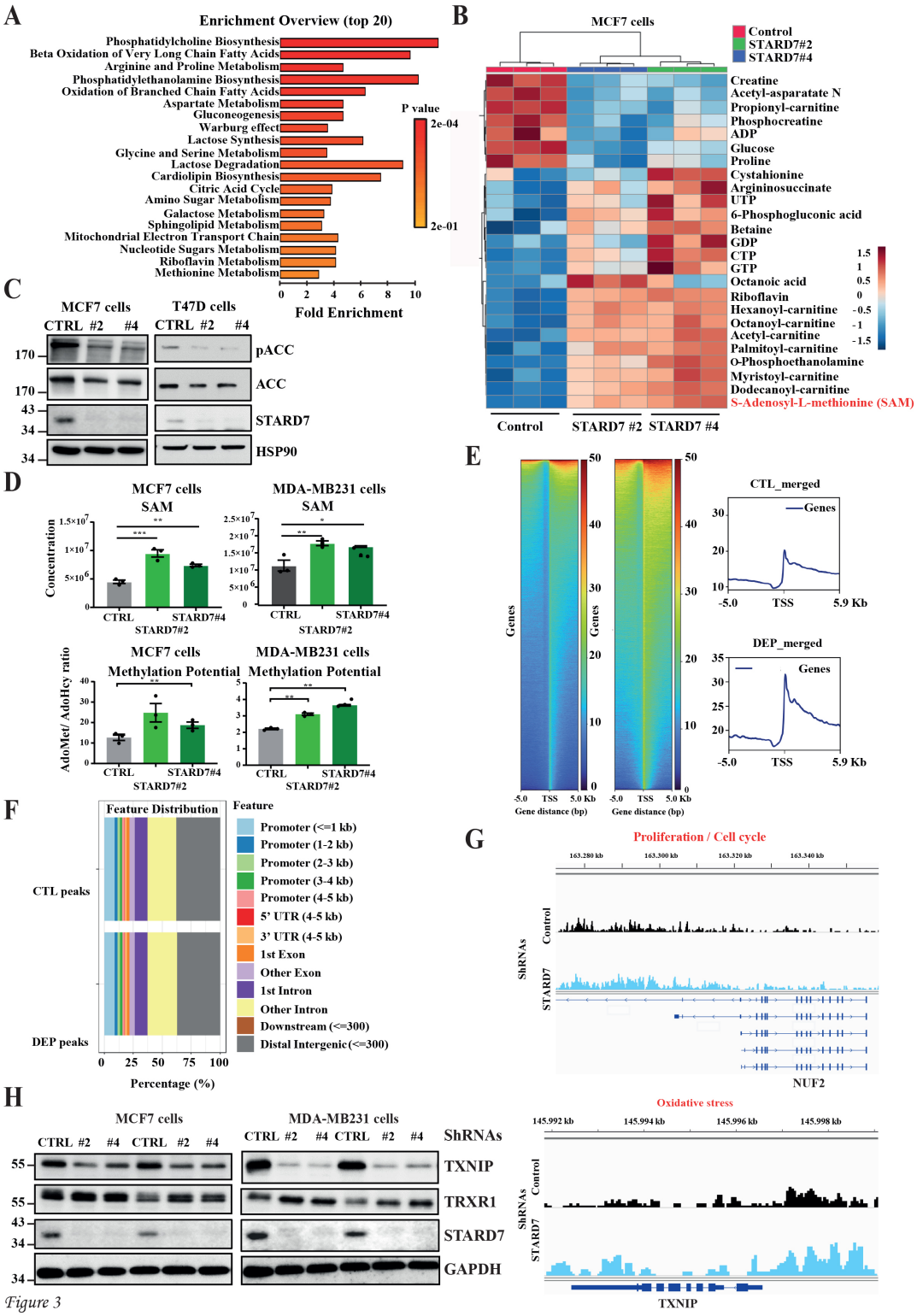


*Figure 3*

## Figure 3

**STARD7 deficiency leads to a metabolic and an epigenetic-mediated transcriptional reprogramming.** **A.**The metabolic signature of both control and STARD7-depleted MCF7 cells was established (see methods for details). An Enrichment overview was conducted and the top 20 upregulated pathways in cells lacking STARD7 are illustrated. **B.** Enrichment of Carnitine derivatives and S-Adenosyl-L-methionine (SAM) in breast cancer cells lacking STARD7. A HeatMap was generated using the metabolomic data

from control and STARD7-depleted MCF7 cells. Metabolites whose level dramatically change upon STARD7 deficiency are illustrated. **C.**Defective ACC expression upon STARD7 deficiency in breast cancer cells. Extracts from both MCF7 and T47D cells were subjected to western blot analyses using the indicated antibodies. **D.**Enhanced SAM levels and methylation potential in breast cancer cells lacking STARD7. The plotted data were extracted from the metabolomic data. * = $p < 0.05$, ** = $p < 0.01$, *** = $p < 0.001$). **E.** and **F.** Enrichment of H3K27 trimethylation on candidates involved in cell proliferation and in the response to oxidative stress. H3K27me3 ChIP-seq analysis of control and STARD7-depleted MCF7 cells (Sh Control, « CTL » and sh STARD7#2, « DEP », respectively) were conducted. Peak profiles and heatmaps depicting genome-wide H3K27me3 peaks aligned by intensity of reads surrounding the TSS (n = 3 merged experiments) are illustrated (E). Color key indicates relative intensity of peaks. Annotated feature distribution of H3K27me3 peaks in control and STARD7-depleted MCF7 cells (« CTL » and « DEP », respectively) within respective genomic regions are shown (F). **G.** Gene tracks of H3K27me3 enrichment on NUF2 and TXNIP genes, respectively (n = 3 merged experiments). TSS-transcription start site. **H.** Downregulation of TXNIP upon STARD7 deficiency in breast cancer cells. Extracts from control and STARD7-depleted MCF7 and MDA-MB231 cells were subjected to western blot analyses using the indicated antibodies.

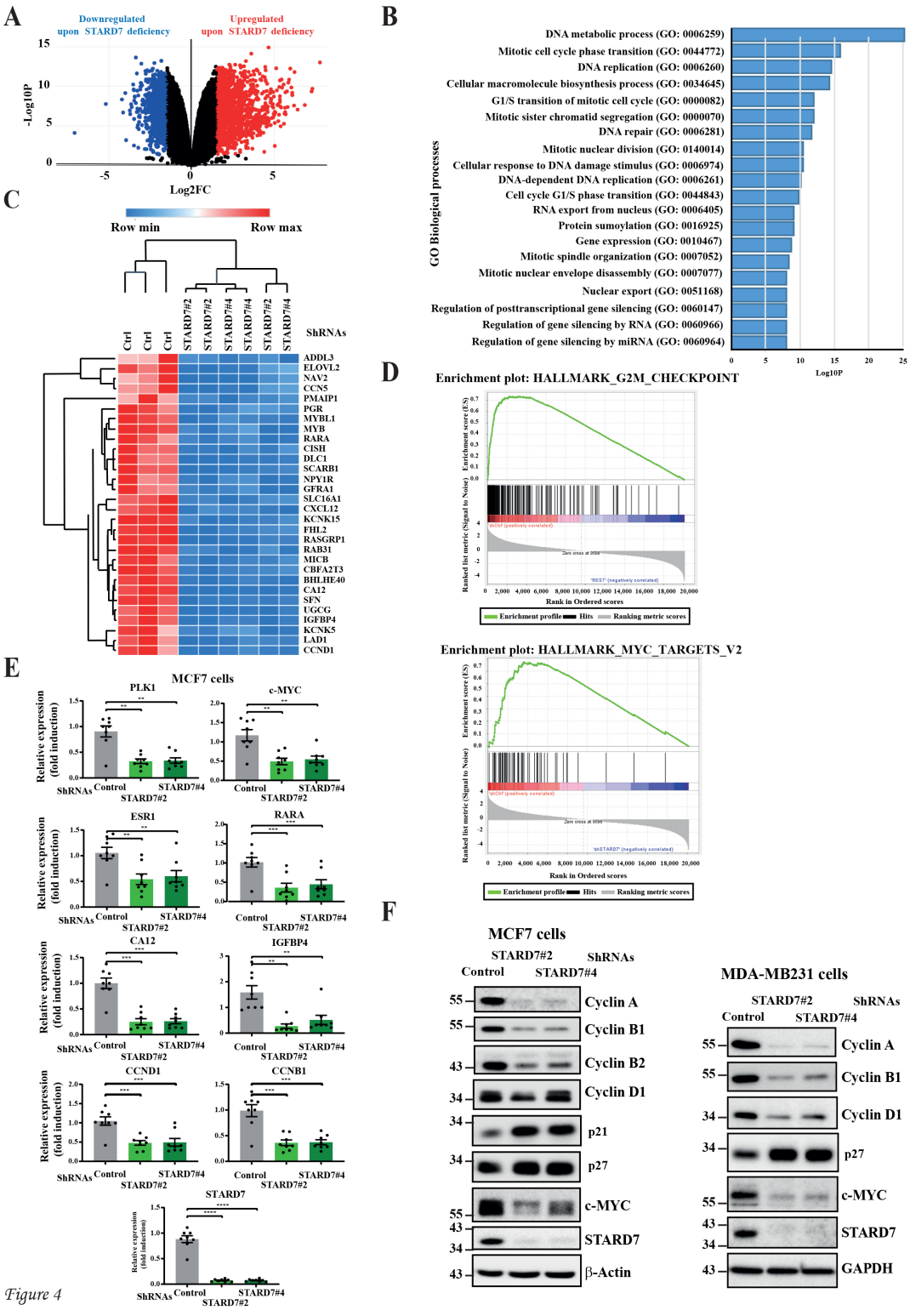


*Figure 4*

## Figure 4

**STARD7 deficiency in breast cancer cells leads to defects in cell cycle progression. A.** Deregulated transcriptional signature in breast cancer cells lacking STARD7. A volcano plot illustrating the up and downregulated candidates (blue and red dots, respectively) upon STARD7 deficiency in MCF7 cells. **B.** STARD7 deficiency causes cell cycle defects in breast cancer cells. A Gene Ontology for biological processes was carried out with transcriptomic data obtained with control versus STARD7-depleted

MCF7 cells. **C.** Top 30 candidates downregulated upon STARD7 deficiency in breast cancer cells. A HeatMap showing the most downregulated candidates in MCF7 cells lacking STARD7 is shown. **D.** STARD7 deficiency impairs the expression of candidates involved in G2M checkpoint as well as c-Myc targets. GSEA were carried out with transcriptomic data obtained with control versus STARD7-depleted MCF7 cells. **E.**and **F.** Impaired expression of candidates involved in cell cycle progression in breast cancer cells lacking STARD7. Real-Time PCR analyses were conducted with total RNAs from control and STARD7-depleted MCF7 cells (E). The expression of each candidate in control cells was set to 1 and levels in cells lacking STARD7 was relative to that after normalization with HSP90 mRNA levels (mean +/- SEM, one-way ANOVA with Dunnettes post test, * = $p < 0.05$, ** = $p < 0.01$, *** = $p < 0.001$, **** = $p < 0.0001$). Extracts from control and STARD7-depleted MCF7 cells were subjected to western blot analyses using the indicated antibodies (F).

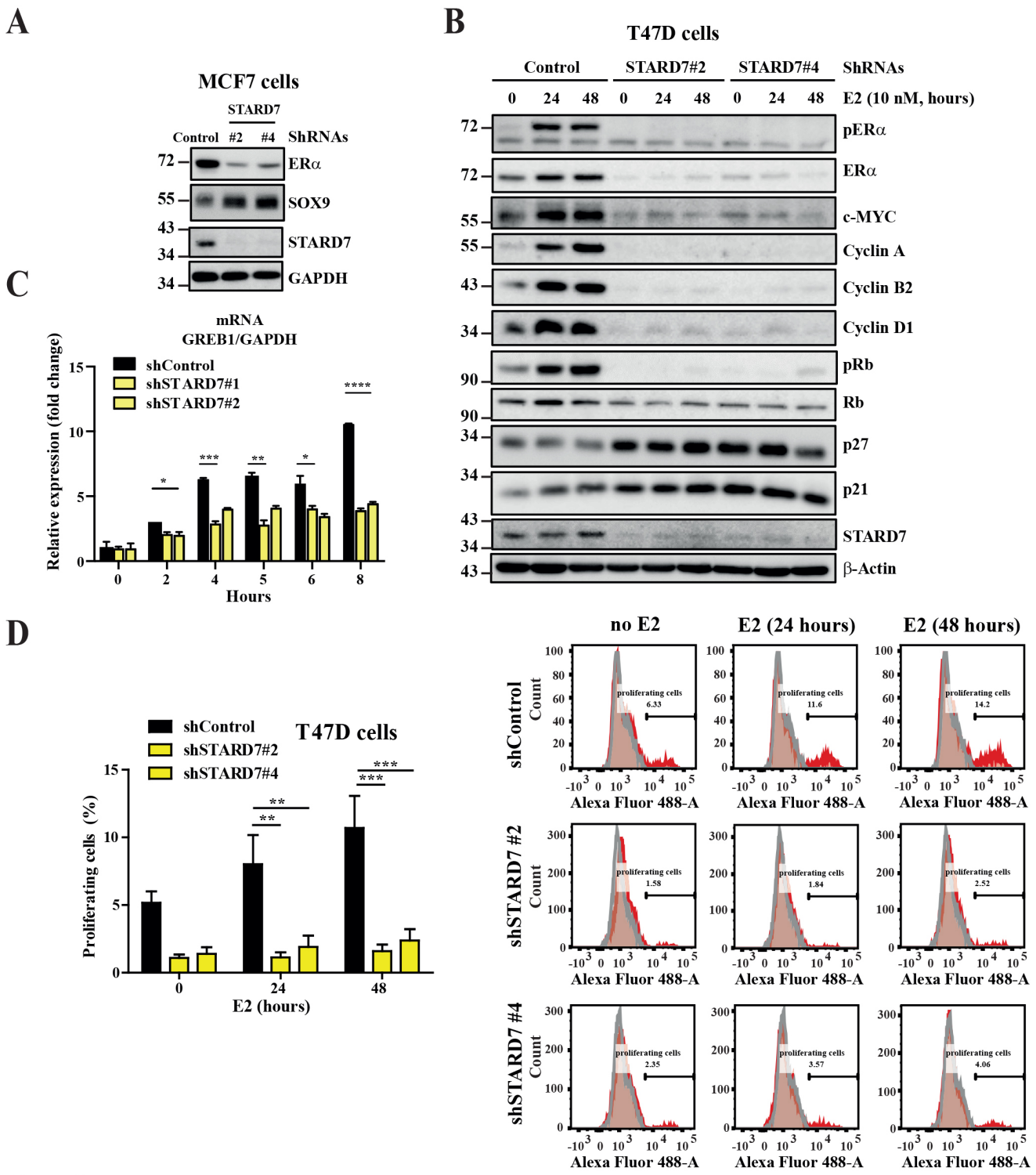


*Figure 5*

## Figure 5

**STARD7 deficiency in breast cancer cells impairs ERa signaling. A.** Impaired ERa expression upon STARD7 deficiency in breast cancer cells. Extracts from control and STARD7-depleted MCF7 cells were subjected to western blot analyses using the indicated antibodies. **B.** Impaired estrogen-dependent signaling upon STARD7 deficiency in breast cancer cells. Control and STARD7-depleted T47D cells incubated in 5 % charcoal-treated serum were treated or not with estrogens (E2, 10 nM) for the indicated

periods of time and the resulting extracts were subjected to western blot (WB) analyses using the indicated antibodies. **C.** Impaired induction of GREB1 by estrogens in breast cancer cells lacking STARD7. Serum-starved control and STARD7-depleted T47D cells were treated or not with E2 (10 nM) for the indicated hours and the resulting extracts were subjected to Real-Time PCR analyses. mRNA levels of GREB1 in untreated control cells were set to 1 and levels in other experimental conditions were relative to that after normalization with GAPDH levels (mean +/- SD, two-way ANOVA, * = $p < 0.05$, ** = $p < 0.01$, *** = $p < 0.001$, **** = $p < 0.0001$). **D.** STARD7 deficiency in breast cancer cells impairs cell proliferation induced by estrogens. Control and STARD7-depleted T47D cells incubated in 5 % charcoal-treated serum were treated or not with E2 (10 nM) for the indicated hours and the resulting cells were subjected to FACS analyses to quantify the percentage of proliferative cells (mean +/- SEM, two-way ANOVA with Dunnettes post test ** = $p < 0.01$, *** = $p < 0.001$).

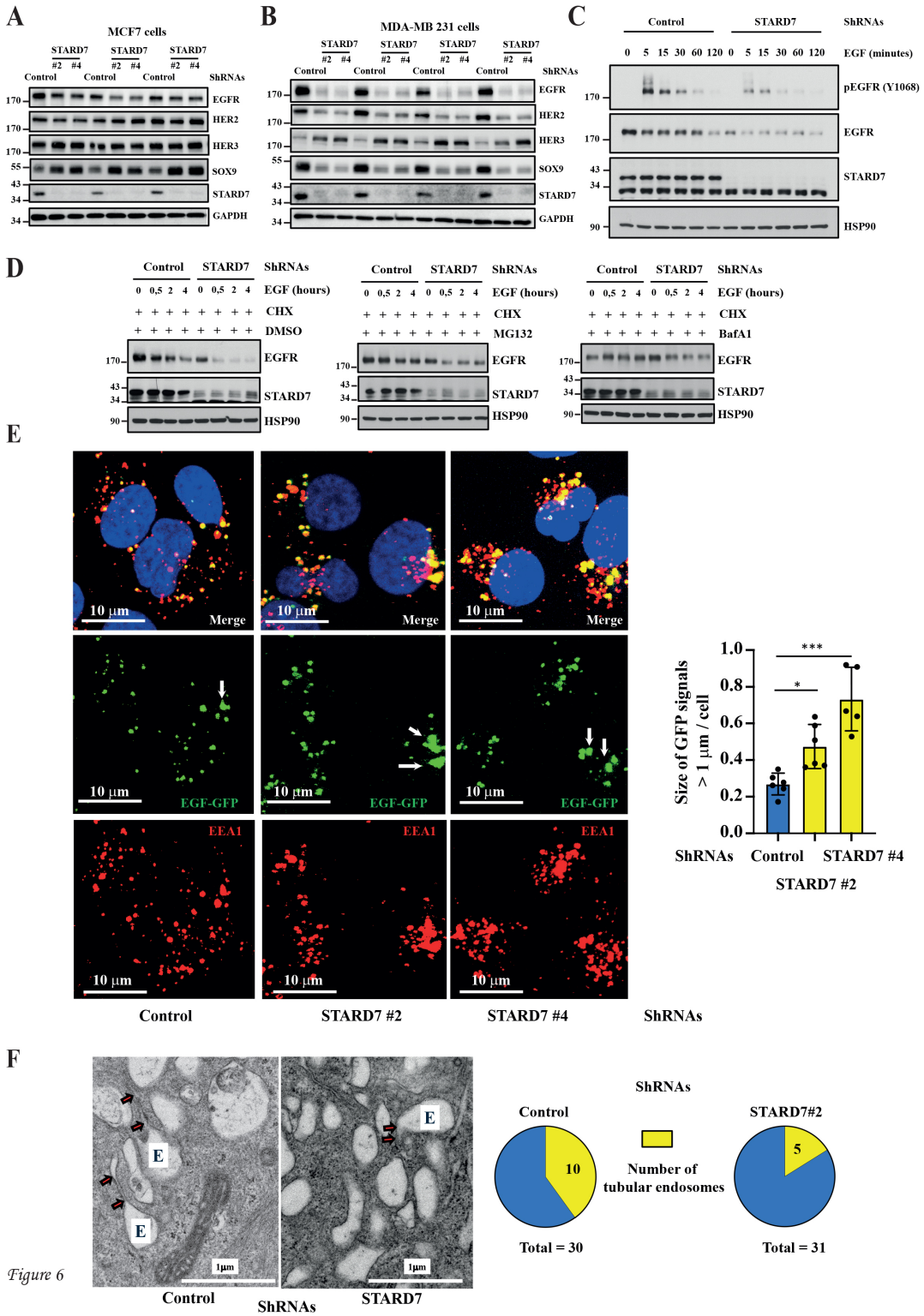


*Figure 6*

## Figure 6

**STARD7 deficiency impairs EGFR signaling. A.** and **B.** STARD7 deficiency impairs EGFR expression in TNBC- but not in ER$^{+}$-derived breast cancer cells. Control and STARD7-depleted MCF7 (A) or MDA-MB-231 (B) cells were subjected to WB analyses using the indicated antibodies. Cell extracts were collected 5 days post-infection. **C.** EGFR signaling relies on STARD7 in TNBC-derived breast cancer cells. Serum-starved control and STARD7-depleted MDA-MB-231 cells were treated or not with EGF (100 nM) for the

indicated periods of time and the resulting extracts were subjected to western blot analyses using the indicated antibodies. Cell extracts were collected 12 days post-infection. **D.** STARD7 deficiency enhances EGFR degradation through lysosomes. Control or STARD7-depleted MDA-MB-231 cells were pretreated with Cycloheximide (CHX, 50 mg/ml) and with DMSO (vehicle), MG132 (25 mM) or Bafilomycin A1 (BafA1) (0.1 mM) for 2 hours and subsequently subjected or not to EGF for the indicated periods of time. The resulting cell extracts were subjected to western blot analyses. **E.** Enlarged early endosomes in breast cancer cells lacking STARD7. Control or STARD7-deficient MDA-MB231 cells were serum starved and subsequently untreated or stimulated with EGF for 30 minutes and subjected to immunofluorescence analyses. EGF-bound to EGFR (green) as well as $EEA1^+$ endosomes (red) were detected. Nuclei were visualized by DAPI stainings. On the right, a quantification of enlarged (> 1 mm) $EEA1^+$ endosomes per cell in EGF-stimulated control and STARD7-depleted cells is illustrated. 6 fields for each experimental condition were analysed (314, 325 and 232 cells for shRNAs Control, STARD7#2 and STARD7#4, respectively) (One-way ANOVA, p-values: ***< 0.001; p-values: *< 0.05). **F.** STARD7 deficiency decreases the number of endosomes with tubular structures. Electron micrographs showing endosomes (E) with tubular structures (arrows) in control versus STARD7-depleted cells are shown. Around thirty photos were randomly taken in both control and STARD7-depleted cells at the level of endosomes at a magnification of 10,000.

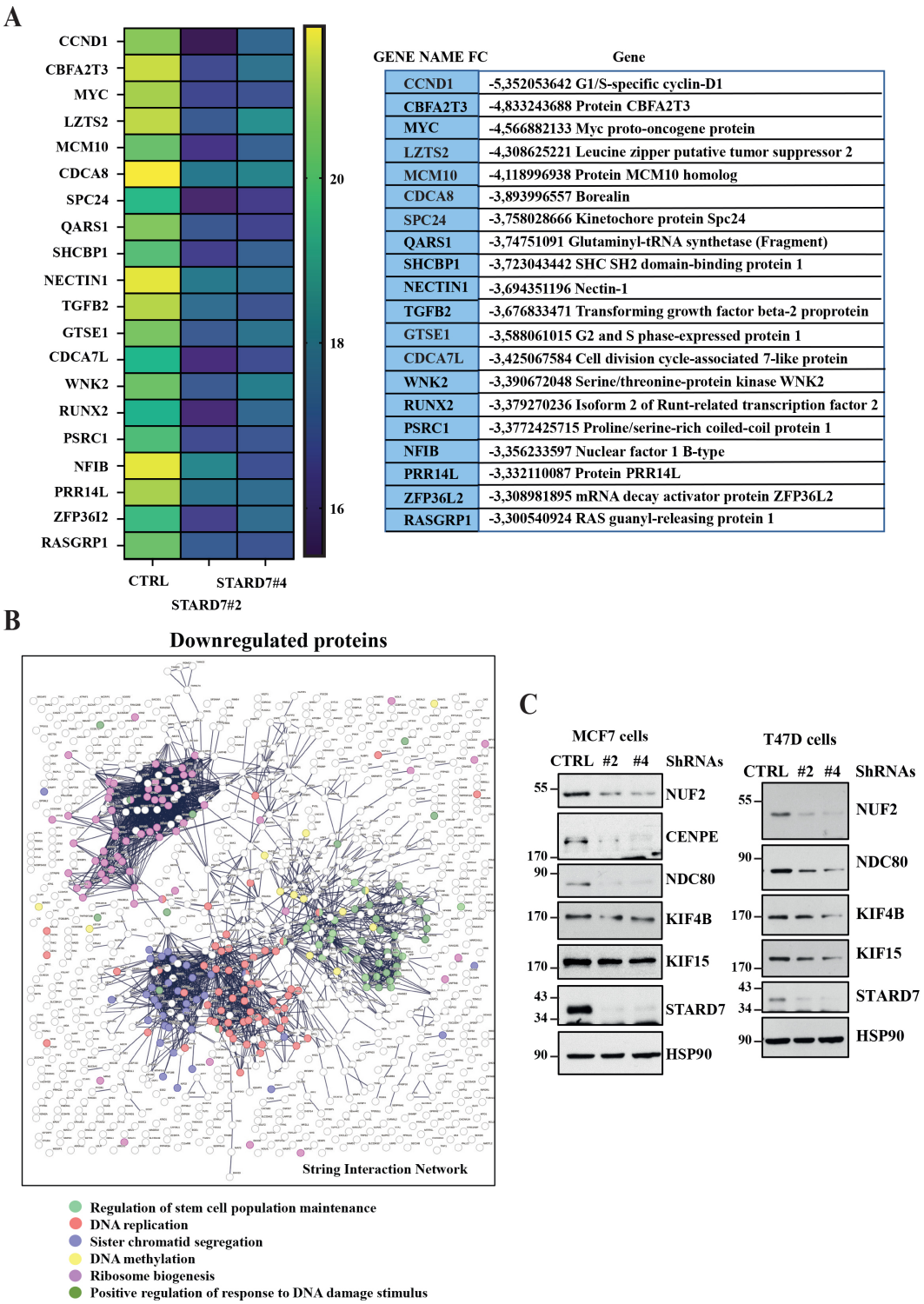


| GENE NAME FC | Gene |
|---|---|
| CCND1 | -5,352053642 G1/S-specific cyclin-D1 |
| CBFA2T3 | -4,833243688 Protein CBFA2T3 |
| MYC | -4,566882133 Myc proto-oncogene protein |
| LZTS2 | -4,308625221 Leucine zipper putative tumor suppressor 2 |
| MCM10 | -4,118996938 Protein MCM10 homolog |
| CDCA8 | -3,893996557 Borealin |
| SPC24 | -3,758028666 Kinetochore protein Spc24 |
| QARS1 | -3,74751091 Glutaminyl-tRNA synthetase (Fragment) |
| SHCBP1 | -3,723043442 SHC SH2 domain-binding protein 1 |
| NECTIN1 | -3,694351196 Nectin-1 |
| TGFB2 | -3,676833471 Transforming growth factor beta-2 proprotein |
| GTSE1 | -3,588061015 G2 and S phase-expressed protein 1 |
| CDCA7L | -3,425067584 Cell division cycle-associated 7-like protein |
| WNK2 | -3,390672048 Serine/threonine-protein kinase WNK2 |
| RUNX2 | -3,379270236 Isoform 2 of Runt-related transcription factor 2 |
| PSRC1 | -3,3772425715 Proline/serine-rich coiled-coil protein 1 |
| NFIB | -3,356233597 Nuclear factor 1 B-type |
| PRR14L | -3,332110087 Protein PRR14L |
| ZFP36L2 | -3,308981895 mRNA decay activator protein ZFP36L2 |
| RASGRP1 | -3,300540924 RAS guanyl-releasing protein 1 |

*Figure 7*

## Figure 7

**STARD7 promotes the expression of candidates involved in DNA replication in breast cancer cells.** **A.**HeatMap of differentially expressed candidates upon STARD7 deficiency in MCF7 cells (proteomic analysis). **B.**STARD7 controls the expression of candidates involved in DNA replication. A String Interaction Network was established with data from proteomic analysis carried out with extracts from control and STARD7-depleted MCF7 cells. **C.** STARD7 promotes the expression of candidates involved in

kinetochore formation. Protein extracts from control and STARD7-depleted MCF7 cells were subjected to western blot analyses using the indicated antibodies.

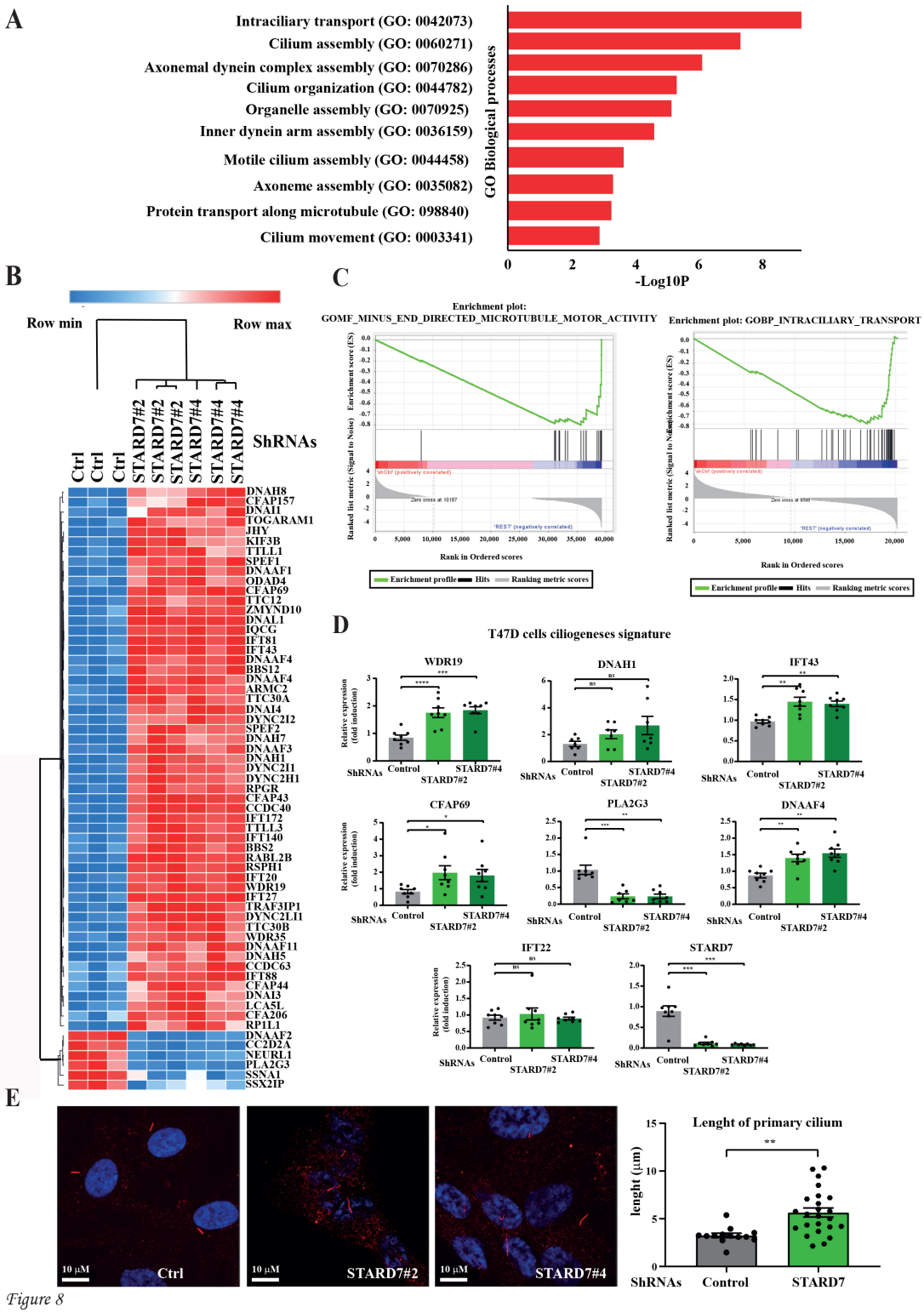


*Figure 8*

## Figure 8

**STARD7 deficiency potentiates ciliogenesis. A.** A ciliogenesis signature is found in breast cancer cells lacking STARD7. A Gene Ontology for biological processes was carried out with RNA Seq data from control and STARD7-depleted MCF7 cells. **B.** Identification of a ciliogenesis signature upon STARD7

deficiency in breast cancer cells. A HeatMap generated with data from the RNA Sequencing experiments is shown. The most differentially expressed candidates between control and STARD7-depleted MCF7 cells are illustrated. **C.** STARD7 deficiency is linked to ciliogenesis. Gene Set Enrichement analyses (GSEA) were carried out with data from RNA Sequencing experiments. **D.**Enhanced mRNA levels of ciliogenesis genes in breast cancer cells lacking STARD7. Real-Time PCR analyses were carried out with total RNAs from control and STARD7-depleted MCF7 cells. mRNA levels of the indicated candidates were set to 1 in control cells and levels in other experimental conditions were relative to that after normalization with HSP90 levels (mean +/- SEM, one-way ANOVA with Dunnetts post test, * = $p < 0.05$, ** = $p < 0.01$, *** = $p < 0.001$, **** = $p < 0.0001$). **E.**Enhanced ciliogenesis upon STARD7 deficiency. Immunofluorescence analyses were carried out with control and STARD7-depleted hTERT-RPE1 cells using the anti-Arl13b to visualize the primary cilium. The length of the primary cilium in control and STARD7-depleted cells was quantified (histogram on the right) (mean +/-SEM, unpaired T-test, ** $p < 0.01$) (see methods for details).

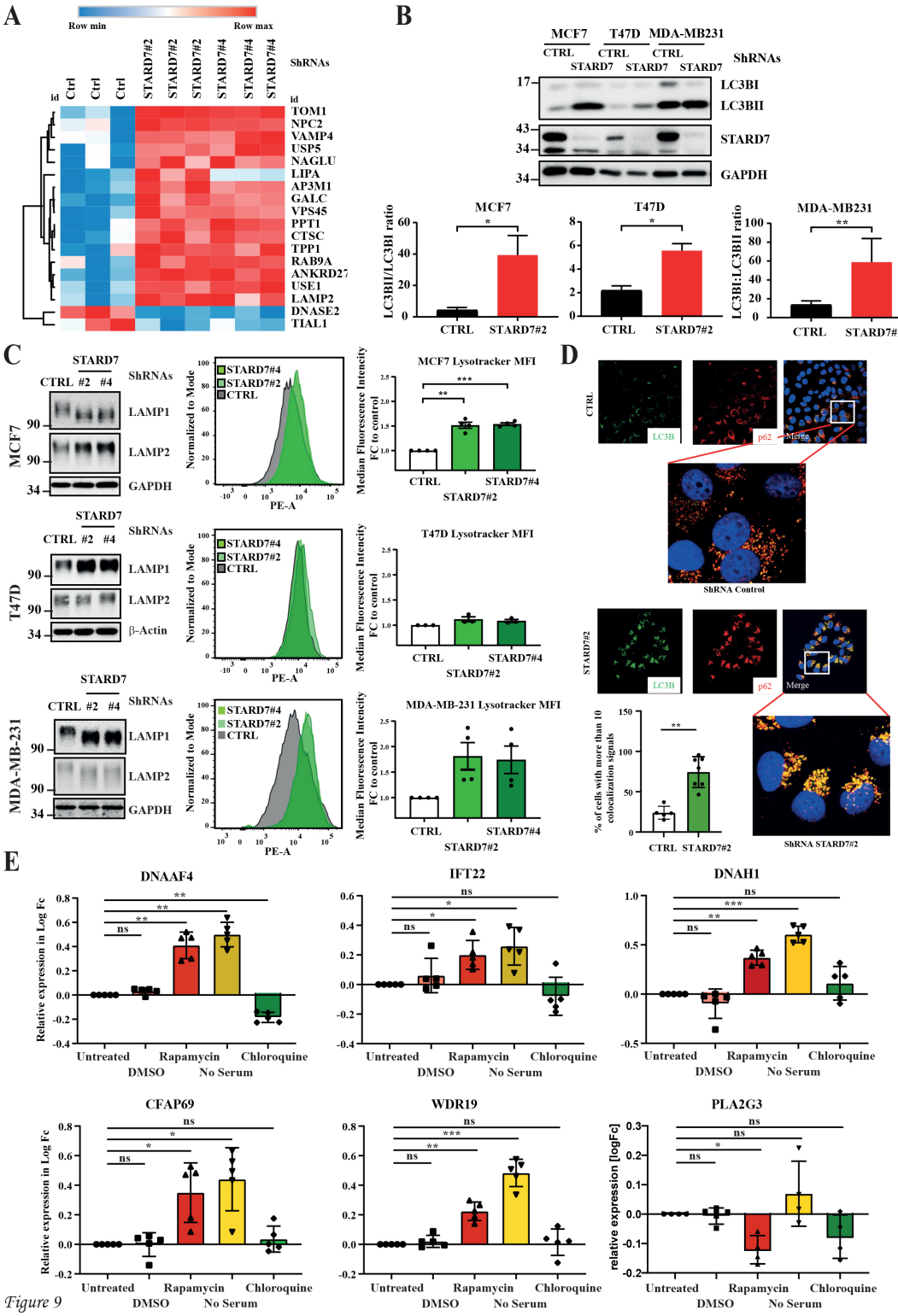


*Figure 9*

## Figure 9

**STARD7 deficiency leads to autophagy. A.** Enrichment of lysosomal proteins in breast cancer cells lacking STARD7. A Heatmap of proteins involved in GO: Lysosome 0005764 was generated with data from control and STARD7-depleted MCF7 cells. Data was obtained from proteomics analysis, hierarchical clustering on raws was performed using one minus pearson's correlation with average linkage method. Relative coloring scheme was applied. **B.** Enhanced levels of the conjugated form of

LC3B in breast cancer cells lacking STARD7. On the top, extracts from the indicated breast cancer cell lines were subjected to western blot analyses using the indicated antibodies. At the bottom, histograms showing the LCB3I/LCB3II (unconjugated and conjugated forms of LC3B, respectively) ratio after Chloroquine (25 mM) overnight treatment. Ratios were calculated for at least 3 independent experiments (mean +/- SEM, paired T-test, * = p < 0.05, ** = p < 0.01). **C.** Enhanced autophagy in breast cancer cells lacking STARD7. On the left, extracts from control and STARD7-depleted MCF7, T47D and MDA-MB231 cells were subjected to western blot analyses using the indicated antibodies. In the middle, FACS analyses using the lysotracker die to monitor autophagy in control and STARD7-depleted breast cancer cells. On the right, histograms illustrating the quantification of FACS data using the lysotracker. The median fluorescence intensity was set to 1 in control cells and values in other experimental conditions were relative to that (mean +/- SEM, one-way ANOVA with Dunnetts post test, * = p < 0.05, ** = p < 0.01, *** = p <0.001). **D.** STARD7 deficiency causes autophagy in breast cancer cells. Representative immunofluorescence analyses of control and STARD7-depleted MCF7 cells (shRNA Control and ShRNA STARD7#2) after an overnight treatement with Chloroquine (15 mM). Anti-p62 (red) and -LC3B stainings were carried out. DAPI was used for nuclei stainings. The bar graph shows a quantitative analysis of cells undergoing autophagy. The quantification shows the percentage of cells with more than 10 co-localized points to the total number of analysed cells (Student T-test, ** = p < 0.01). **E.**The ciliogenesis signature of breast cancer cells lacking STARD7 results from autophagy. MCF7 cells were treated or not with DMSO (vehicle), Rapamycin (20 nM), Chloroquine (25 mM) or were serum-starved and mRNA levels of the indicated candidates were quantified by Real-Time PCR analyses (mean +/- EM, one-way ANOVA with Dunnetts post test, * = p < 0.05, ** = p < 0.01, *** = p <0.001).

## Supplementary Files

This is a list of supplementary files associated with this preprint. Click to download.

- SupplementaryInformation.docx
- Uncroppedgels.pdf